

# Toward a new theory of the fractional quantum Hall effect:

## I. What is the ground state of a quantum Hall system at $\nu = 1/3$ ?

S. A. Mikhailov\*

*Institute of Physics, University of Augsburg, D-86135 Augsburg, Germany*

(Dated: October 27, 2023)

The fractional quantum Hall effect was experimentally discovered in 1982. It was observed that the Hall conductivity  $\sigma_{yx}$  of a two-dimensional electron system is quantized,  $\sigma_{yx} = e^2/3h$ , in the vicinity of the Landau level filling factor  $\nu = 1/3$ . In 1983, Laughlin proposed a many-body variational wave function, which he claimed described a “new state of matter” – a homogeneous incompressible liquid with fractionally charged quasi-particles. Here I develop an exact diagonalization theory that makes it possible to calculate the energy and other physical properties of the ground and excited states of a system of  $N$  two-dimensional Coulomb interacting electrons in a strong magnetic field and in the field of a compensating positively charged background. The only assumption of the theory is that all electrons occupy only the lowest Landau level. I present results for  $N \leq 7$  and show that the true ground state resembles a sliding Wigner crystal. I also calculate the physical properties of the  $\nu = 1/3$  Laughlin state for  $N \leq 8$  and show that properties of the “Laughlin liquid” differ significantly from those of the true ground state. In addition, I show that the variational principle that was used for the estimate of the Laughlin state energy in the thermodynamic limit does not prove the validity of the wave function, since one can specify an infinitely large number of different trial wave functions giving the same variational energy at  $N \rightarrow \infty$ . This work represents the first step toward a new theory of the fractional quantum Hall effect.

## CONTENTS

I. Introduction	2
A. Historical background	2
B. Brief overview of results of this paper	3
II. Theory	5
A. Single-particle problem	5
B. Positive background	6
C. Many-body Hamiltonian	6
D. Basis many-body wave functions	7
E. Many-body matrix elements	8
1. Electron density	9
2. Fourier transform of the electron density	9
3. Background-background interaction energy	9
4. Background-electron interaction energy	10
5. Electron-electron interaction energy	10
6. Pair correlation function	11
F. General solution of the many-body Schrödinger problem	12
III. Exact solution	12
A. Classical Wigner crystal configurations	12
B. Ground state energy and wave function	14
C. Density of electrons in the ground state	16
D. Pair correlation function in the ground state	17
IV. Maximum density droplet state, $\nu = 1$	17
A. Wave function	17
B. Energy of an $N$ -particle system	17
C. Electron density	19

---

\* Electronic mail: sergey.mikhailov@physik.uni-augsburg.de

D. Pair correlation function	19
E. Thermodynamic limit	20
V. Laughlin wave function at $\nu = 1/3$	21
A. General remarks	21
B. Expansion coefficients of the Laughlin function	22
1. Two particles	22
2. Three particles	23
3. Four particles	23
4. Five to eight particles	23
C. Energy of the Laughlin state	24
D. Deviation of the Laughlin wave function from the true ground state wave function	25
E. Electron density in the Laughlin state	26
F. Pair correlation function in the Laughlin state	27
G. Additional remark to the case of $N = 7$ particles	28
H. About the variational principle in the thermodynamic limit	28
I. Electron density in the Laughlin state at large $N$	29
J. Final remarks	33
VI. Summary and conclusions	34
Acknowledgments	34
A. Matrix elements of the background-electron interaction energy	34
1. General formulas	34
2. Maximum density droplet state	35
B. Integrals $\mathcal{K}$	36
C. Supplementary Materials	36
References	37

## I. INTRODUCTION

### A. Historical background

The quantum Hall effect was discovered by Klaus von Klitzing in 1980 [1]. He studied the longitudinal ( $R_{xx}$ ) and Hall ( $R_H = R_{xy}$ ) resistances of a degenerate two-dimensional (2D) electron gas (EG) in the inversion layer of a Si-MOSFET (metal-oxide-semiconductor field effect transistor). The sample was placed in a strong perpendicular magnetic field  $B \approx 18$  T and cooled down to  $T \approx 1.5$  K. The resistances  $R_{xx}$  and  $R_{xy}$  were measured as a function of the gate voltage  $V_g$ , applied between the metallic gate and the 2DEG, which changed the density  $n_s$  of 2D electrons and the Landau level filling factor

$$\nu = \pi n_s \lambda^2; \quad (1)$$

here

$$\lambda = \sqrt{\frac{2\hbar c}{|e|B}} = \sqrt{\frac{2\hbar}{m^* \omega_c}}, \quad (2)$$

$\omega_c = |e|B/m^*c$  is the cyclotron frequency, and  $m^*$  is the effective mass of electrons ( $\lambda/\sqrt{2} \equiv l_B$  is the magnetic length). He found that, when  $\nu$  is close to integer values  $\nu \approx i$ ,  $i = 1, 2, 3, \dots$ , the diagonal resistance  $R_{xx}$  becomes negligibly small, while the Hall resistance takes on, with a very high accuracy, quantized values, corresponding to the Hall conductivity

$$\sigma_{yx} = \frac{e^2}{h} \nu = \frac{e^2}{h} i, \quad i = 1, 2, 3, \dots \quad (3)$$

The origin of this fascinating physical phenomenon, which was called the *integer quantum Hall effect*, was quickly understood [1] in terms of the single-particle picture. Landau quantization of electron motion leads to the appearance of energy gaps in the electron spectrum when  $\nu \approx i$ ; the classical formula for the Hall conductivity  $\sigma_{yx} = n_s e c/B$ , together with the relation (1) immediately gives the quantized values (3). The stabilization of  $\sigma_{yx}$  at the levels (3) and the vanishing of  $\sigma_{xx}$  in finite intervals around  $\nu = i$  was explained by the influence of disorder, see, e.g., Ref. [2].

The time of mysteries came a little later. In 1982 Tsui, Stormer and Gossard published a paper [3] where the same transport coefficients ( $R_{xx}$  and  $R_{xy}$ ) were measured in another material system, GaAs/AlGaAs heterojunction. The main difference between the new experiment and the one of von Klitzing was that the mobility of 2D electrons was higher ( $\mu \sim 10^5$  cm<sup>2</sup>/Vs) and the temperature was lower ( $T$  down to  $\sim 0.48$  K). In the experiment [3] the density of electrons was fixed while the magnetic field varied from zero up to  $\sim 22$  T. Like in Ref. [1], the already familiar integer quantization of  $R_{xy}$  was observed around  $\nu = 1, 2, 3, \dots$ , but – very surprisingly – a very similar plateau was found around  $\nu \approx 1/3$ , where the measured  $R_H$  corresponded to the Hall conductivity

$$\sigma_{yx} = \frac{e^2}{h} \nu, \quad \nu = \frac{1}{3}. \quad (4)$$

Subsequent experimental studies showed that such a *fractional* quantization of  $\sigma_{yx}$  and the corresponding suppression of  $\sigma_{xx}$  is the case around many fractions of the form  $\nu = p/q$  where  $p$  and  $q$  are integers and  $q$  is odd, see, e.g., Fig. 1 in Ref. [4].

If  $\nu < 1$ , all electrons occupy the highly degenerate lowest Landau level, and there are no energy gaps in the single-particle electron spectrum. Therefore the mysterious feature at  $\nu = 1/3$  could be explained only within a many-body approach, taking into account electron-electron interactions. As known, when considered as classical point particles, Coulomb-interacting electrons form the Wigner crystal [5], and Tsui et al. [3] put forward a hypothesis that the observed 1/3 feature in the Hall conductivity is related to the formation of the Wigner crystal (or a charge density wave) with a triangular symmetry. However, in 1983 Robert Laughlin [6] proposed the following variational wave function for the ground state of the  $N$ -particle system at  $\nu = 1/m$ :

$$\Psi_{\text{RL}}^m(\mathbf{r}_1, \mathbf{r}_2, \dots, \mathbf{r}_N) \propto \left( \prod_{1 \leq j < k \leq N} (z_j - z_k)^m \right) \exp \left( -\frac{1}{2} \sum_{j=1}^N |z_j|^2 \right); \quad (5)$$

here  $m$  is odd integer,  $\mathbf{r}_j = (x_j, y_j)$ , and  $z_j = (x_j - iy_j)/\lambda$  are the normalized complex coordinates of 2D electrons. The function  $\Psi_{\text{RL}}^m$  is the eigenfunction of the total angular momentum operator with the eigenvalue  $\mathcal{L} = mN(N-1)/2$  (in units of  $\hbar$ ). If  $m = 1$ , it coincides with the wave function of the so called maximum density droplet (MDD) state proposed earlier in Ref. [7] for the ground state of the system at  $\nu = 1$ . The MDD state is characterized by a uniform electron density at  $r \lesssim R = \sqrt{N/\pi n_s}$ , see Section IV for further details.

For  $m = 3$  and 5 Laughlin calculated the energy of the state (5) in the thermodynamic limit and found that it is lower than the energy of the charge density wave evaluated in Refs. [8, 9] using the Hartree-Fock [8] and second-order perturbation theory [9]. He also evaluated projections of the wave function (5) with  $m = 3$  and 5 onto the numerically calculated exact ground state for  $N = 3$  and 4, and found them to be close to 1. He suggested that elementary excitations of the liquid (5) are quasi-particles with fractional charges, and concluded that the wave function (5) describes the ground state of the system at  $\nu = 1/m$  and is “a new state of matter”, which represents “an incompressible quantum fluid with fractionally charged excitations” [6]. A few critical comments on the wave function (5) followed [10], and several more attempts have been made to find an alternative ground state of the fractional quantum Hall effect (FQHE) system [11, 12], but finally the state (5) was accepted by the community [13] as the closest approximation to the ground-state wave function at  $\nu = 1/m$  (with  $m = 3$  and 5). The Laughlin ideas have been developed in a very large number of subsequent publications, for example, Refs. [14–22]. Reports on the experimental observations of fractionally charged quasi-particles were published in Refs. [23–25]. Some reviews articles can be found in Refs. [26–29].

## B. Brief overview of results of this paper

In this paper, I present an exact diagonalization theory that makes it possible to calculate the energy and other physical properties of the ground and excited states of a system of  $N$  two-dimensional Coulomb interacting electrons in a strong magnetic field and in the field of a neutralizing positively charged background having the shape of a disk of the radius  $R = \sqrt{N/\pi n_s}$  and the constant areal density  $n_s$ . The theory is developed under the assumption that all electrons are spin-polarized and occupy only the lowest Landau level states. This assumption implies that the typical

Coulomb interaction energy  $e^2/a_0$  should be smaller than the inter-Landau-level distance  $\hbar\omega_c$ ,

$$\frac{e^2/a_0}{\hbar\omega_c} \ll 1, \quad \text{or} \quad \nu \ll 2\sqrt{\pi n_s a_B^2} = 2\frac{a_B}{a_0}; \quad (6)$$

here  $a_0 = 1/\sqrt{\pi n_s}$  is the average distance between electrons and  $a_B = \hbar^2/m^*e^2$  is the effective Bohr radius (I do not explicitly write the dielectric permittivity of the environment  $\epsilon$  in formulas containing Coulomb forces and energies; to restore it, one should just replace  $e^2 \rightarrow e^2/\epsilon$ ). If  $\nu \simeq 1/3$ , the condition (6) is satisfied in GaAs/AlGaAs heterostructures ( $a_B \simeq 10$  nm) at typical 2DEG densities  $n_s \simeq 3 \times 10^{11}$  cm $^{-2}$ . If  $\nu \simeq 1$ , then it holds for  $n_s \gtrsim 10^{12}$  cm $^{-2}$ , so that at lower densities one would have to take states from higher Landau levels into account.

Under the assumptions made, the problem is reduced to the diagonalization of a large but finite size Hamiltonian matrix, all elements of which are calculated analytically. Specific calculations are performed using Wolfram Mathematica, which allows one to get results for energy and other physical properties of the system with very high accuracy, for any  $\nu < 1$  and, in principle, any number of particles  $N$ .

Calculations for very large  $N$  are limited by the amount of available computer memory and the allowable computation time. In this paper, I present exact results for the ground and the lowest excited states of the systems with  $N \leq 7$  electrons, for  $\nu = 1/3$ . These calculations show that the true ground state has the form resembling a sliding Wigner crystal, in that sense that maxima of the electron density calculated quantum-mechanically coincide with positions of electrons in the classical Wigner molecule. I also calculate the physical properties of the  $\nu = 1/3$  Laughlin state (5) for  $N \leq 8$ , and show that there exists a very large discrepancy, growing with  $N$ , between the properties of the “Laughlin liquid” (5) and those of the true ground state. In particular,

- at  $N = 7$ , the energy of the Laughlin state (5), counted from the energy of the true ground state  $E_{\text{GS}}$ ,  $E_{\text{RL}} - E_{\text{GS}}$ , is almost six times greater than the energy difference  $E_{1\text{st}} - E_{\text{GS}}$  between the true first excited state and the true ground state:  $(E_{\text{RL}} - E_{\text{GS}})/(E_{1\text{st}} - E_{\text{GS}}) = 5.8825\ldots$ ;
- the standard deviation of the Laughlin wave function from the true ground state wave function exceeds 40% at  $N = 7$ ;
- the difference in electron densities in the center of the disk between the Laughlin state and the true ground state reaches  $\sim 70\%$  at  $N = 7$ ;
- the pair correlation function of the Laughlin state  $P_{\text{RL}}(\mathbf{r}, \mathbf{r}')$  differs from the pair correlation function of the true ground state  $P_{\text{GS}}(\mathbf{r}, \mathbf{r}')$  by many orders of magnitude when the distance  $|\mathbf{r} - \mathbf{r}'|$  becomes smaller than  $\sim 0.3a_0$ .

The above results are obtained for a system consisting of a finite number of particles. To defend the Laughlin wave function (5), one usually argues that it always “wins” in the thermodynamic limit: As was shown in Ref. [6], the function (5) gives the lowest energy per particle at  $N \rightarrow \infty$ ,  $E_{\text{RL}}/N = -0.4156e^2/l_B$  at  $\nu = 1/3$ , compared to all other trial functions. However, it is easy to prove that this argument does not hold water.

Assume that the true ground ( $s = 1$ ) and excited ( $s = 2, 3, \dots$ ) states of the system are known. Their energies and the wave functions are  $E_s$  and  $\Psi_s$ . Let a trial wave function be a linear combination of the ground ( $\Psi_1 \equiv \Psi_{\text{GS}}$ ) and several low-lying excited states,

$$\Psi_{\text{trial}} = \alpha_1 \Psi_{\text{GS}} + \sum_{s>1} \alpha_s \Psi_s. \quad (7)$$

The energy of the trial state  $E_{\text{trial}}$  will then be

$$E_{\text{trial}} = \alpha_1^2 E_{\text{GS}} + \sum_{s>1} \alpha_s^2 E_s = E_{\text{GS}} + \sum_{s>1} \alpha_s^2 (E_s - E_{\text{GS}}), \quad (8)$$

where the normalization condition  $\sum_s \alpha_s^2 = 1$  is taken into account.

The energy differences between the low-lying excited states and the ground state  $E_s - E_{\text{GS}}$  do not depend on  $N$  and are determined by typical energies of the FQHE problem,  $e^2/a_0$ ,  $e^2/l_B$ , or  $\hbar\omega_c$ , which are on the meV scale. But the energy  $E_{\text{GS}}$  is proportional to the number of particles  $N$  and tends to minus infinity in the thermodynamic limit. Under typical experimental conditions ( $N \simeq 10^{11}$ ) it is on the GeV scale. Therefore, the energy per particle in the limit  $N \rightarrow \infty$  will be the same both for the true ground state and *for any* trial wave function:

$$\lim_{N \rightarrow \infty} \frac{E_{\text{trial}}}{N} = \lim_{N \rightarrow \infty} \frac{E_{\text{GS}}}{N} + \sum_{s>1} \alpha_s^2 \lim_{N \rightarrow \infty} \frac{E_s - E_{\text{GS}}}{N} = \lim_{N \rightarrow \infty} \frac{E_{\text{GS}}}{N}. \quad (9)$$

This conclusion holds also in the case  $\alpha_1 = 0$ , i.e., when the trial and the ground state wave functions are orthogonal. In Section V G I give an example where the Laughlin function is orthogonal to the true ground state wave function. Thus, while the “thermodynamic limit” argument may give a correct estimate for the ground state energy per particle, it completely fails to determine the correct ground state wave function. In Section V H I discuss it in more detail and provide some specific examples.

It should be noted that the conclusion that the Laughlin function is not suitable for the role of the ground state wave function of the system could have been made many years ago. In Refs. [18, 19] exact diagonalization studies of the FQHE problem were performed for  $N = 9$  [18] and  $N = 16$  [19] particles. However, in both papers the physical properties (electron density, pair correlation function) of the exact ground and Laughlin states were not investigated and compared. The authors only analyzed the convergence of the exact energy per particle to the Laughlin value in the thermodynamic limit, which could not help in identifying the true ground state wave function of the system, as shown here.

Thus, the quantum-mechanical variational principle, that perfectly works for one- or few-particle systems, is useless in the limit  $N \rightarrow \infty$ . Relying on this principle, one can mistakenly take any arbitrarily unreasonable wave function as a correct ground state wave function. This conclusion is general and applies not only to the Laughlin state and the FQHE problem, but also to other many body problems in which attempts have been made to find the ground state of a macroscopic system using trial wave functions. Conclusions about the nature of the ground state of the system must thus be drawn from (ideally exact) solutions obtained for a finite number of electrons. My exact diagonalization results, as well as results of some other authors (e.g., Refs. [18, 20, 21], see a detailed discussion below), show that the Laughlin state has nothing to do with the true ground state of the system.

The rest of the paper is organized as follows. Section II is preparatory. Here I formulate the problem and discuss all the technical issues needed for the remaining part of the paper; in particular, I calculate the many-particle matrix elements of the Hamiltonian and other physical quantities. In Section III I perform an exact diagonalization study of the problem for  $2 \leq N \leq 7$  and present the results for the energies of the exact ground and some excited states, as well as for the electron density and the pair correlation function. Section IV is devoted to the analysis of the maximum density droplet state, a special case of the Laughlin wave function at  $m = 1$ . In Section V I calculate the energy and other physical properties of the Laughlin trial state (5) for  $m = 3$ , and compare them with the exact results from Section III. In Section VI I summarize the results and formulate the conclusions. Mathematical details are given in the Appendices. The Supplementary Materials contain information which will help the reader to reproduce and verify the results obtained.

## II. THEORY

### A. Single-particle problem

Consider a single 2D electron moving in the plane  $z = 0$  in the presence of a uniform external magnetic field  $\mathbf{B} = (0, 0, B)$ . Its quantum-mechanical motion is described by the single-particle Schrödinger equation

$$\frac{1}{2m^*} \left( \hat{\mathbf{p}} + \frac{|e|}{2c} \mathbf{B} \times \mathbf{r} \right)^2 \phi(\mathbf{r}) = \epsilon \phi(\mathbf{r}). \quad (10)$$

Its solution,

$$\epsilon \equiv \epsilon_{n,l} = \hbar\omega_c \left( n + \frac{l + |l| + 1}{2} \right), \quad 0 \leq n < \infty, \quad -\infty < l < +\infty, \quad (11)$$

$$\phi(\mathbf{r}) \equiv \phi_{n,l}(\mathbf{r}) = \frac{e^{il\theta}}{\sqrt{\pi\lambda}} \left( \frac{n!}{(n + |l|)!} \right)^{1/2} \exp \left( -\frac{r^2}{2\lambda^2} \right) \left( \frac{r}{\lambda} \right)^{|l|} L_n^{|l|} \left( \frac{r^2}{\lambda^2} \right), \quad (12)$$

is characterized by the radial quantum number  $n$  and the azimuthal (angular momentum) quantum number  $l$ . The functions (12) represent a complete basis set in a 2D space.

The states with  $n = 0$  and non-positive  $l$ ,  $l \leq 0$ , belong to the lowest Landau level. The corresponding energy equals  $\hbar\omega_c/2$  and the corresponding wave functions are

$$|L\rangle \equiv \psi_L(\mathbf{r}) \equiv \phi_{n=0,l \leq 0}(\mathbf{r}) = \frac{1}{\lambda\sqrt{\pi L!}} \left( \frac{r}{\lambda} e^{-i\theta} \right)^L \exp \left( -\frac{r^2}{2\lambda^2} \right) = \frac{z^L e^{-|z|^2/2}}{\lambda\sqrt{\pi L!}}, \quad (13)$$

where  $L = -l = 0, 1, 2, \dots$ , and  $z = (x - iy)/\lambda$ . The states (13) are normalized,  $\langle L|L' \rangle = \delta_{LL'}$ , and represent a complete subset of functions in two dimensions belonging to the lowest Landau level with  $\epsilon_{0,l} = \hbar\omega_c/2$ . The matrix elements of the exponential function  $e^{i\mathbf{q} \cdot \mathbf{r}}$  between the single-particle states (13) are

$$\langle L|e^{i\mathbf{q} \cdot \mathbf{r}}|L'\rangle = i^{|L-L'|} e^{i(L-L')\alpha} \sqrt{\frac{(\min\{L, L'\})!}{(\max\{L, L'\})!}} \left(\frac{q\lambda}{2}\right)^{|L-L'|} \exp\left(-\frac{(q\lambda)^2}{4}\right) L_{\min\{L, L'\}}^{|L-L'|} \left(\frac{(q\lambda)^2}{4}\right), \quad (14)$$

where  $\alpha$  is the polar angle of the vector  $\mathbf{q}$ ,  $\mathbf{q} = q(\cos \alpha, \sin \alpha)$ , and  $L_n^l(x)$  are the Laguerre polynomials.

### B. Positive background

$N$  electrons repel each other by Coulomb forces, therefore a compensating positive background is required to keep them together and to ensure the system electroneutrality. As in Refs. [6, 20–22], I assume that the positive background has the shape of a disk with a uniform charge density  $n_s$  and a radius  $R = \sqrt{N/\pi n_s}$ ,

$$n_b(\mathbf{r}) = n_s \Theta(R - r) = n_s \Theta(\sqrt{N} - x). \quad (15)$$

Here  $x = r/a_0$ ,  $\Theta(x)$  is the Heaviside step function, and the length  $a_0$ , defined as

$$\pi n_s a_0^2 = 1, \quad (16)$$

will be used as the length unit throughout the paper. In contrast to other possible options for choosing the length unit (e.g.,  $l_B$  or  $\lambda$ , as was done in Refs. [6, 16, 20–22]),  $a_0$  does not depend on  $B$ , which is more convenient for the system behavior analysis at varying magnetic fields (e.g., at different  $m$ , see discussion in Section VI).

In order to calculate physical properties of the system I will need Fourier transforms of the background density profile. Calculations give

$$n_{\mathbf{q}}^b \equiv \int d\mathbf{r} n_b(\mathbf{r}) e^{i\mathbf{q} \cdot \mathbf{r}} = N \frac{J_1(qR)}{qR/2} = 2N \frac{J_1(Q\sqrt{N})}{Q\sqrt{N}}, \quad (17)$$

where  $Q = qa_0$  and  $J_1$  is the Bessel function. The potential energy created by the positively charged background disk (15) is described by the formula

$$V_b(\mathbf{r}) = \frac{e^2}{a_0} U_N \left(\frac{r}{a_0}\right), \quad (18)$$

where

$$U_N \left(\frac{r}{a_0}\right) = -\frac{4}{\pi} \sqrt{N} \left\{ \begin{array}{l} E(\zeta^2), \\ \zeta E(\zeta^{-2}) - (\zeta - 1/\zeta) K(\zeta^{-2}), \end{array} \right. \begin{array}{l} \zeta \leq 1 \\ \zeta \geq 1 \end{array}, \quad \zeta = \frac{r}{a_0 \sqrt{N}} = \frac{r}{R}, \quad (19)$$

and the functions  $K(m)$  and  $E(m)$ , defined as

$$K(m) = \int_0^{\pi/2} \frac{d\theta}{\sqrt{1 - m \sin^2 \theta}}, \quad E(m) = \int_0^{\pi/2} d\theta \sqrt{1 - m \sin^2 \theta}, \quad (20)$$

are complete elliptic integrals of the first and second kind, respectively. Figure 1 shows the potential energy (19) for  $N = 7$ . The depth of the potential well (18) grows with  $N$  as  $\sqrt{N}$ ,  $V_b(\mathbf{0}) = -2\sqrt{N}(e^2/a_0)$ .

### C. Many-body Hamiltonian

The Hamiltonian of  $N$  interacting 2D electrons, placed in the attractive potential (18) of the positive background (15) and in the magnetic field  $\mathbf{B} = (0, 0, B)$ , has the form

$$\hat{\mathcal{H}} = \hat{K} + \hat{V}_C = \frac{1}{2m} \sum_{j=1}^N \left( \hat{\mathbf{p}}_j + \frac{|e|}{2c} \mathbf{B} \times \mathbf{r}_j \right)^2 + \hat{V}_C. \quad (21)$$

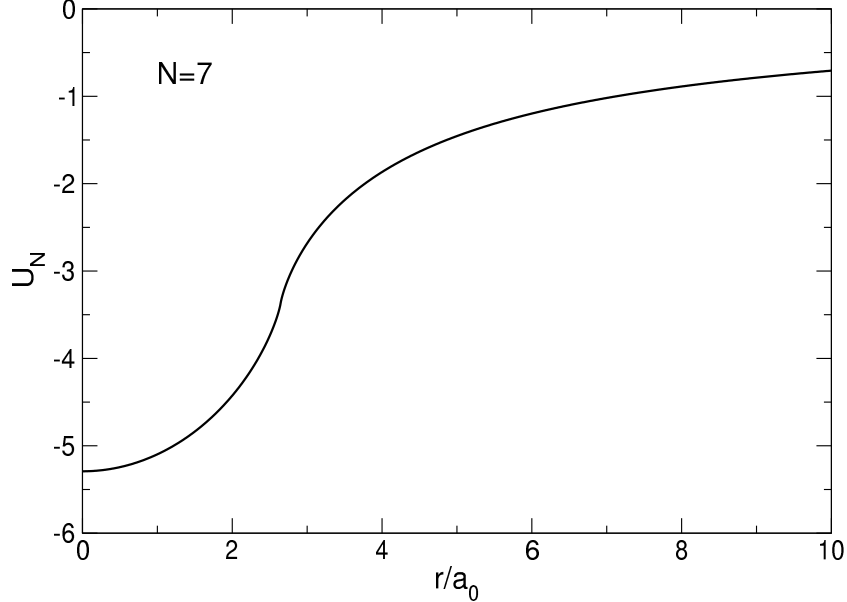


FIG. 1. The potential energy (19) of the positive background with the density profile (15) for  $N = 7$ .

Here  $\hat{K}$  is the total kinetic energy operator and the Coulomb interaction energy  $\hat{V}_C = \hat{V}_{bb} + \hat{V}_{eb} + \hat{V}_{ee}$  consists of the sum of background-background, background-electron and electron-electron interaction energies,

$$\hat{V}_C = \frac{e^2}{2} \int \frac{n_b(\mathbf{r})n_b(\mathbf{r}')d\mathbf{r}d\mathbf{r}'}{|\mathbf{r} - \mathbf{r}'|} - e^2 \int n_b(\mathbf{r})d\mathbf{r} \sum_{j=1}^N \frac{1}{|\mathbf{r} - \mathbf{r}_j|} + \frac{e^2}{2} \sum_{j \neq k=1}^N \frac{1}{|\mathbf{r}_j - \mathbf{r}_k|}. \quad (22)$$

In order to calculate the energy  $\hat{V}_C$  it is convenient to rewrite (22) in terms of Fourier transforms of the electron and background charge densities. This gives

$$\hat{V}_C = \frac{e^2}{2\pi} \int \frac{d\mathbf{q}}{q} \left( \frac{1}{2} (n_{\mathbf{q}}^b)^2 - n_{\mathbf{q}}^b \sum_{j=1}^N e^{-i\mathbf{q} \cdot \mathbf{r}_j} + \frac{1}{2} \sum_{j \neq k=1}^N e^{i\mathbf{q} \cdot \mathbf{r}_j} e^{-i\mathbf{q} \cdot \mathbf{r}_k} \right), \quad (23)$$

where  $n_{\mathbf{q}}^b$  is given by Eq. (17). The Hamiltonian (21) commutes with the total angular momentum operator

$$\hat{\mathcal{L}}_z = \sum_{j=1}^N (\mathbf{r}_j \times \hat{\mathbf{p}}_j)_z. \quad (24)$$

The total angular momentum quantum number  $\mathcal{L} \equiv \mathcal{L}_z$  can be used to classify the many-body basis wave functions.

#### D. Basis many-body wave functions

Consider  $N$  spin-polarized electrons at the lowest Landau level. Each of the particles can occupy one of the states (13). If the  $j$ -th particle is in the single-particle state  $|L_j\rangle = \psi_{L_j}(\mathbf{r})$ , the corresponding many-body wave function can be written as a Slater determinant

$$|L_1, L_2, \dots, L_N\rangle = \frac{1}{\sqrt{N!}} \begin{vmatrix} \psi_{L_1}(\mathbf{r}_1) & \psi_{L_1}(\mathbf{r}_2) & \dots & \psi_{L_1}(\mathbf{r}_N) \\ \psi_{L_2}(\mathbf{r}_1) & \psi_{L_2}(\mathbf{r}_2) & \dots & \psi_{L_2}(\mathbf{r}_N) \\ \dots & \dots & \dots & \dots \\ \psi_{L_N}(\mathbf{r}_1) & \psi_{L_N}(\mathbf{r}_2) & \dots & \psi_{L_N}(\mathbf{r}_N) \end{vmatrix}. \quad (25)$$

The functions (25) are orthogonal and normalized,

$$\langle L'_1, L'_2, \dots, L'_N | L_1, L_2, \dots, L_N \rangle = \delta_{L'_1 L_1} \delta_{L'_2 L_2} \dots \delta_{L'_N L_N}. \quad (26)$$

They are eigenfunctions of the kinetic energy operator

$$\hat{K}|L_1, L_2, \dots, L_N\rangle = N \frac{\hbar\omega_c}{2} |L_1, L_2, \dots, L_N\rangle, \quad (27)$$

and of the total angular momentum operator  $\hat{\mathcal{L}}$

$$\hat{\mathcal{L}}_z|L_1, L_2, \dots, L_N\rangle = \left( \sum_{i=1}^N L_i \right) |L_1, L_2, \dots, L_N\rangle, \quad (28)$$

where the latter is measured in units of  $\hbar$ . The many-body wave functions (25) represent the orthonormal basis set of functions belonging to the lowest Landau level.

If  $N$  electrons occupy the single-particle states with the lowest possible angular momenta  $L$  from  $L = 0$  up to  $L = N - 1$ , one gets the many-body configuration  $\Psi_{\text{mdd}} = |0, 1, 2, \dots, N - 1\rangle$ , Ref. [7], which is often referred to as the maximum density droplet (MDD) state. This MDD configuration has the lowest possible total angular momentum

$$\mathcal{L} = \mathcal{L}_{\min} = \sum_{L=0}^{N-1} L = \frac{N(N-1)}{2}. \quad (29)$$

If  $\mathcal{L} > \mathcal{L}_{\min}$ , there exist, in general, more than one many-body electronic configurations corresponding to the given  $N$  and  $\mathcal{L}$ . For example, Tables I and II show possible many-body configurations for  $N = 2$  and  $N = 3$  and several  $\mathcal{L}$ . The number  $N_{\text{mbs}}(N, \mathcal{L})$  of many-body configurations grows with  $\mathcal{L}$  for a given  $N$ .

TABLE I. Possible many-body configurations in a system of  $N = 2$  electrons.  $N_{\text{mbs}}(N, \mathcal{L})$  is the total number of all many-particle configurations with given  $N$  and  $\mathcal{L}$ .

$\mathcal{L}$	Configurations	$N_{\text{mbs}}$
1	$ 0, 1\rangle$	1
2	$ 0, 2\rangle$	1
3	$ 0, 3\rangle  1, 2\rangle$	2
4	$ 0, 4\rangle  1, 3\rangle$	2
5	$ 0, 5\rangle  1, 4\rangle  2, 3\rangle$	3
6	$ 0, 6\rangle  1, 5\rangle  2, 4\rangle$	3
7	$ 0, 7\rangle  1, 6\rangle  2, 5\rangle  3, 4\rangle$	4

TABLE II. Possible many-body configurations in a system of  $N = 3$  particles.  $N_{\text{mbs}}(N, \mathcal{L})$  is the total number of all many-particle configurations with given  $N$  and  $\mathcal{L}$ .

$\mathcal{L}$	Configurations	$N_{\text{mbs}}$
3	$ 0, 1, 2\rangle$	1
4	$ 0, 1, 3\rangle$	1
5	$ 0, 1, 4\rangle  0, 2, 3\rangle$	2
6	$ 0, 1, 5\rangle  0, 2, 4\rangle  1, 2, 3\rangle$	3
7	$ 0, 1, 6\rangle  0, 2, 5\rangle  0, 3, 4\rangle  1, 2, 4\rangle$	4
8	$ 0, 1, 7\rangle  0, 2, 6\rangle  0, 3, 5\rangle  1, 2, 5\rangle  1, 3, 4\rangle$	5
9	$ 0, 1, 8\rangle  0, 2, 7\rangle  0, 3, 6\rangle  0, 4, 5\rangle  1, 2, 6\rangle  1, 3, 5\rangle  2, 3, 4\rangle$	7

### E. Many-body matrix elements

For calculation of different physical properties of an  $N$ -electron system I will need matrix elements of one-particle or two-particle operators,

$$\langle L'_1, L'_2, \dots, L'_N | \sum_{j=1}^N \hat{F}_1(\mathbf{r}_j) |L_1, L_2, \dots, L_N\rangle, \quad (30)$$

$$\langle L'_1, L'_2, \dots, L'_N | \sum_{j=1}^N \sum_{k=1, k \neq j}^N \hat{F}_2(\mathbf{r}_j, \mathbf{r}_k) | L_1, L_2, \dots, L_N \rangle, \quad (31)$$

with the many-body states (25). In this paper I will consider only the ground state properties of the system. In this case I will need only the matrix elements (30)–(31) between the many-body states  $\langle L'_1, L'_2, \dots, L'_N |$  and  $| L_1, L_2, \dots, L_N \rangle$ , belonging to the same total angular momentum  $\mathcal{L}$ , i.e.,  $\sum_{j=1}^N L_j = \sum_{j=1}^N L'_j = \mathcal{L}$ . This means that, if the bra and ket configurations are different, they differ by two or more single-particle states, for example,  $\langle 0, 1, 8 |$  and  $| 0, 2, 7 \rangle$ ,  $\langle 0, 3, 6 |$  and  $| 1, 3, 5 \rangle$  (configurations differ by two single-particle states),  $\langle 0, 1, 8 |$  and  $| 2, 3, 4 \rangle$  (configurations differ by three single-particle states), etc., see Table II. The matrix elements between the bra and ket configurations which differ by only one single-particle state, e.g., between the configurations  $\langle 0, 1, 8 |$  and  $| 0, 1, 9 \rangle$ , will not be considered since they correspond to different values of the total angular momentum  $\mathcal{L}$ .

Now I calculate matrix elements of several one-particle and two-particle operators of the type (30)–(31). For brevity I will use the short notations  $|s\rangle \equiv |\Psi_s\rangle \equiv |L_1^{(s)}, L_2^{(s)}, \dots, L_N^{(s)}\rangle$  for the functions (25).

### 1. Electron density

The operator of the electron density has the form

$$\hat{n}_e(\mathbf{r}) = \sum_{j=1}^N \delta(\mathbf{r} - \mathbf{r}_j). \quad (32)$$

The off-diagonal matrix elements of (32) are evidently zero. Then one gets

$$\langle \Psi_s | \hat{n}_e(\mathbf{r}) | \Psi_{s'} \rangle = \delta_{ss'} \sum_{j=1}^N \langle L_j^{(s)} | \delta(\mathbf{r} - \mathbf{r}_j) | L_j^{(s)} \rangle = \delta_{ss'} \sum_{j=1}^N |\psi_{L_j^{(s)}}(\mathbf{r})|^2, \quad (33)$$

where  $\psi_{L_j^{(s)}}(\mathbf{r})$  is the single-particle wave function (13) of the  $j$ -th particle in the  $s$ -th many-body configuration.

### 2. Fourier transform of the electron density

The Fourier transform of the density operator (32) is

$$\hat{n}_{\mathbf{q}}^e = \int d\mathbf{r} \hat{n}_e(\mathbf{r}) e^{i\mathbf{q} \cdot \mathbf{r}} = \sum_{j=1}^N e^{i\mathbf{q} \cdot \mathbf{r}_j}. \quad (34)$$

Using Eq. (14) I get

$$\langle \Psi_s | \hat{n}_{\mathbf{q}}^e | \Psi_{s'} \rangle = \delta_{ss'} \sum_{j=1}^N \langle L_j^{(s)} | e^{i\mathbf{q} \cdot \mathbf{r}_j} | L_j^{(s)} \rangle = \delta_{ss'} \exp\left(-\frac{(q\lambda)^2}{4}\right) \sum_{j=1}^N L_{L_j^{(s)}}^0\left(\frac{(q\lambda)^2}{4}\right). \quad (35)$$

### 3. Background-background interaction energy

The background-background interaction energy  $V_{bb}$  is given by the first term in Eq. (23). Since  $V_{bb}$  does not depend on the coordinates of electrons, the matrix  $\langle \Psi_s | \hat{V}_{bb} | \Psi_{s'} \rangle$  is diagonal and all matrix elements are the same. In the case of the step-like density profile (15) they are

$$\langle \Psi_s | \hat{V}_{bb} | \Psi_{s'} \rangle = \delta_{ss'} \frac{e^2}{a_0} \frac{8}{3\pi} N^{3/2}. \quad (36)$$

#### 4. Background-electron interaction energy

The background-electron interaction energy is given by the second term in Eq. (23). Its many-body matrix elements are

$$\langle \Psi_s | \hat{V}_{be} | \Psi_{s'} \rangle = -\frac{e^2}{2\pi} \int \frac{d\mathbf{q}}{q} n_{\mathbf{q}}^b \langle \Psi_s | (\hat{n}_{\mathbf{q}}^e)^* | \Psi_{s'} \rangle. \quad (37)$$

Substituting the Fourier transforms of the background and electron densities from Eqs. (17) and (35) into (37) I obtain after some transformations (see Appendix A 1)

$$\langle \Psi_s | \hat{V}_{be} | \Psi_{s'} \rangle = -\delta_{ss'} \frac{e^2}{a_0} N \sqrt{\beta} \sum_{j=1}^N \sum_{m=0}^{L_j^{(s)}} \binom{L_j^{(s)}}{m} \frac{(-1)^m}{m!} \Gamma \left( m + \frac{1}{2} \right) {}_1F_1 \left( m + \frac{1}{2}, 2; -N\beta \right). \quad (38)$$

Here

$$\beta = \frac{a_0^2}{\lambda^2} = \frac{1}{\nu} \quad (39)$$

is the inverse Landau level filling factor,  $\binom{L}{m}$  are the binomial coefficients,  $\Gamma(x)$  is the Gamma function, and  ${}_1F_1(a, b; z)$  is the degenerate (or confluent) hypergeometric function, Eq. (A11). The matrix elements (38) depend on the magnetic field  $B$ .

#### 5. Electron-electron interaction energy

The electron-electron interaction energy is given by the third term in Eq. (23). Calculating its many-body matrix elements I get the following result

$$\langle \Psi_s | \hat{V}_{ee} | \Psi_{s'} \rangle = \delta_{ss'} (V_{ss}^H - V_{ss}^F) + (1 - \delta_{ss'}) V_{ss}^{\text{off}}, \quad (40)$$

where the diagonal matrix elements are given by the difference of Hartree and Fock contributions,

$$V_{ss}^H = \frac{e^2}{2a_0} \int_0^\infty dq a_0 \sum_{i=1}^N \langle L_i^{(s)} | e^{i\mathbf{q} \cdot \mathbf{r}} | L_i^{(s)} \rangle \sum_{j=1}^N \langle L_j^{(s)} | e^{-i\mathbf{q} \cdot \mathbf{r}} | L_j^{(s)} \rangle, \quad (41)$$

$$V_{ss}^F = \frac{e^2}{2a_0} \int_0^\infty dq a_0 \sum_{i=1}^N \sum_{j=1}^N \left| \langle L_i^{(s)} | e^{i\mathbf{q} \cdot \mathbf{r}} | L_j^{(s)} \rangle \right|^2. \quad (42)$$

Substituting here the matrix elements of the exponential functions from Eq. (14) I get

$$V_{ss}^H = \frac{e^2}{a_0} \sqrt{\frac{\pi\beta}{8}} \sum_{j=1}^N \sum_{k=1}^N \mathcal{K}(L_j^{(s)}, L_k^{(s)}, 0), \quad (43)$$

$$V_{ss}^F = \frac{e^2}{a_0} \sqrt{\frac{\pi\beta}{8}} \sum_{j=1}^N \sum_{k=1}^N \mathcal{K}(L_{\min}, L_{\min}, \delta L), \quad (44)$$

where the integrals  $\mathcal{K}$  are defined and calculated in Appendix B; in the last formula

$$L_{\min} = \min\{L_j^{(s)}, L_k^{(s)}\}, \quad L_{\max} = \max\{L_j^{(s)}, L_k^{(s)}\}, \quad \delta L = |L_j^{(s)} - L_k^{(s)}| = L_{\max} - L_{\min}. \quad (45)$$

The formulation of results for the off-diagonal matrix elements ( $s \neq s'$ ) requires a bit longer discussion. First, since  $s \neq s'$ , the sets of numbers  $L_j^s$  and  $L_j^{s'}$ ,  $j = 1, 2, \dots, N$ , differ from each other. In general, these sets may differ by one,

two or more numbers. The case when they differ by only one number is excluded, since both sets should satisfy the total angular momentum conservation condition. If they differ by more than two numbers, the corresponding matrix elements equal zero,

$$\langle \Psi_s | \hat{V}_{ee} | \Psi_{s'} \rangle = 0, \text{ if the sets } L_j^s \text{ and } L_j^{s'} \text{ differ by more than two numbers.} \quad (46)$$

Thus, the matrix elements  $\langle \Psi_s | \hat{V}_{ee} | \Psi_{s'} \rangle$  are nonzero if and only if the states  $|s\rangle$  and  $|s'\rangle$  differ from each other by the single-particle states of exactly two particles. For example, for three particles with the total angular momentum  $\mathcal{L} = 9$ , Table II, the matrix elements

$$\langle 0, 2, 7 | \hat{V}_{ee} | 0, 4, 5 \rangle \text{ and } \langle 0, 1, 8 | \hat{V}_{ee} | 1, 2, 6 \rangle \quad (47)$$

are finite (only two numbers in the bra and ket configurations are different), but the matrix element

$$\langle 0, 2, 7 | \hat{V}_{ee} | 1, 3, 5 \rangle \quad (48)$$

is zero (all three numbers are different).

Let the configurations

$$|s\rangle = | \dots, \underbrace{L_1^s}_{p_1^s}, \dots, \underbrace{L_2^s}_{p_2^s}, \dots \rangle \text{ and } |s'\rangle = | \dots, \underbrace{L_1^{s'}}_{p_1^{s'}}, \dots, \underbrace{L_2^{s'}}_{p_2^{s'}}, \dots \rangle \quad (49)$$

differ from each other by the  $L$ -states of exactly two particles. I designate them as  $L_1^s$ ,  $L_2^s$  and  $L_1^{s'}$ ,  $L_2^{s'}$ , and their serial numbers in the sets  $|s\rangle$  and  $|s'\rangle$  as  $p_1^s$ ,  $p_2^s$ ,  $p_1^{s'}$ ,  $p_2^{s'}$ ; all other states in (49), designated by dots, are identical. For example, for the first of the matrix elements in (47),  $\langle 0, 2, 7 | \hat{V}_{ee} | 0, 4, 5 \rangle$ , these numbers are  $L_1^s = 2$ ,  $L_2^s = 7$ ,  $p_1^s = 2$ ,  $p_2^s = 3$ , and  $L_1^{s'} = 4$ ,  $L_2^{s'} = 5$ ,  $p_1^{s'} = 2$ ,  $p_2^{s'} = 3$ . For the second matrix element in (47),  $\langle 0, 1, 8 | \hat{V}_{ee} | 1, 2, 6 \rangle$ , they are  $L_1^s = 0$ ,  $L_2^s = 8$ ,  $p_1^s = 1$ ,  $p_2^s = 3$ , and  $L_1^{s'} = 2$ ,  $L_2^{s'} = 6$ ,  $p_1^{s'} = 2$ ,  $p_2^{s'} = 3$ .

Now I can formulate the results for the off-diagonal matrix elements of the electron-electron interaction energy. Calculations show that

$$\begin{aligned} V_{ss'}^{\text{off}} &= \frac{e^2}{a_0} \sqrt{\frac{\pi\beta}{2}} (-1)^{p_1^s + p_2^s + p_1^{s'} + p_2^{s'}} \\ &\times \left[ \mathcal{K} \left( \min\{L_1^s, L_1^{s'}\}, \min\{L_2^s, L_2^{s'}\}, |L_1^s - L_1^{s'}| \right) - \mathcal{K} \left( \min\{L_1^s, L_2^{s'}\}, \min\{L_2^s, L_1^{s'}\}, |L_1^s - L_2^{s'}| \right) \right], \\ &\quad s \neq s', \end{aligned} \quad (50)$$

where the integrals  $\mathcal{K}$  are defined in Eq. (B3).

Equations (40), (43), (44) and (50) give the matrix elements of the electron-electron interaction between the basis many-body configurations (25). Notice that the magnetic field enters these formulas only via the common prefactor  $\sqrt{\beta}$ , which means that for all values of  $B$  the  $ee$ -interaction matrix needs to be calculated only once.

### 6. Pair correlation function

The operator of the pair correlation function is defined as

$$\hat{P}(\mathbf{r}, \mathbf{r}') = \sum_{j=1}^N \sum_{k=1, k \neq j}^N \delta(\mathbf{r} - \mathbf{r}_j) \delta(\mathbf{r}' - \mathbf{r}_k). \quad (51)$$

Its diagonal and off-diagonal matrix elements are determined by the following formulas,

$$\langle \Psi_s | \hat{P}(\mathbf{r}, \mathbf{r}') | \Psi_s \rangle = \sum_{j=1}^N \sum_{k=1}^N \left( |\psi_{L_j^{(s)}}(\mathbf{r})|^2 |\psi_{L_k^{(s)}}(\mathbf{r}')|^2 - \psi_{L_j^{(s)}}^*(\mathbf{r}) \psi_{L_k^{(s)}}(\mathbf{r}) \psi_{L_j^{(s)}}(\mathbf{r}') \psi_{L_k^{(s)}}^*(\mathbf{r}') \right), \quad (52)$$

$$\langle \Psi_s | \hat{P}(\mathbf{r}, \mathbf{r}') | \Psi_{s'} \rangle = (-1)^{p_1^s + p_2^s + p_1^{s'} + p_2^{s'}} \left( \psi_{L_1^s}^*(\mathbf{r}) \psi_{L_2^s}^*(\mathbf{r}') \det \begin{vmatrix} \psi_{L_1^{s'}}(\mathbf{r}) & \psi_{L_2^{s'}}(\mathbf{r}) \\ \psi_{L_1^{s'}}(\mathbf{r}') & \psi_{L_2^{s'}}(\mathbf{r}') \end{vmatrix} + (\mathbf{r} \leftrightarrow \mathbf{r}') \right), \quad s \neq s', \quad (53)$$

where the numbers  $L_1^s$ ,  $L_2^s$ ,  $L_1^{s'}$ ,  $L_2^{s'}$ , as well as  $p_1^s$ ,  $p_2^s$ ,  $p_1^{s'}$ ,  $p_2^{s'}$  have the same meaning as in the previous Section.

### F. General solution of the many-body Schrödinger problem

Consider the  $N$ -particle Schrödinger equation

$$\hat{\mathcal{H}}\Psi(\mathbf{r}_1, \mathbf{r}_2, \dots, \mathbf{r}_N) = E\Psi(\mathbf{r}_1, \mathbf{r}_2, \dots, \mathbf{r}_N). \quad (54)$$

In order to solve it for a given total angular momentum  $\mathcal{L}$ , the function  $\Psi$  should be searched in the form of a linear combination of all  $N_{mbs}(N, \mathcal{L})$  many-body configurations corresponding to given values of  $N$  and  $\mathcal{L}$ ,

$$|\Psi\rangle = \sum_{s'=1}^{N_{mbs}} A_{s'} |\Psi_{s'}\rangle. \quad (55)$$

In this formula  $A_s$  are unknown numbers. Substituting (55) into (54) and multiplying the resulting equation by  $\langle \Psi_s |$  one reduces the Schrödinger problem to the matrix equation

$$\sum_{s'=1}^{N_{mbs}} \langle \Psi_s | \hat{\mathcal{H}} | \Psi_{s'} \rangle A_{s'} = EA_s. \quad (56)$$

The size of the Hamiltonian matrix  $\mathcal{H}_{ss'} \equiv \langle \Psi_s | \hat{\mathcal{H}} | \Psi_{s'} \rangle$  here is  $N_{mbs} \times N_{mbs}$ . Solving the eigenvalue problem (56) one can find  $N_{mbs}$  solutions for given  $N$  and  $\mathcal{L}$ : the energies  $E_{N,\mathcal{L},k}$  and the sets of numbers  $A_s^{N,\mathcal{L},k}$ ,  $k = 1, \dots, N_{mbs}$ , which give the corresponding many-body wave functions according to the expansion (55). After the numbers  $A_s^{N,\mathcal{L},k}$  are found one can also calculate all physical properties of the ground or excited many-body states, for example, the electron density and the pair correlation function, using the corresponding matrix elements found in Section II E.

All matrix elements of the Hamiltonian  $\mathcal{H}_{ss'}$  are calculated analytically, see Section II E. As a result, the energies and wave functions of the  $N$ -electron system can be calculated, in principle, with a very high accuracy for any  $\nu \leq 1$  and any  $\mathcal{L}$  and  $N$ . In practice, of course, the computation time becomes too large if  $N$  or  $\mathcal{L}$  are much greater than one. Nevertheless, the ground state physics of a fractional quantum Hall system can be quite well understood even if the number of particles is less than or on the order of ten. Especially valuable are results for  $N = 7$ , because seven spin-polarized electrons form a highly symmetric piece of a macroscopic Wigner crystal, see Figure 2(g) below.

In the next Section I show results of the theory for  $2 \leq N \leq 7$  and the Landau level filling factor  $\nu = 1/3$ . Laughlin suggested [6] that the total angular momentum in the ground state at  $\nu = 1/3$  equals  $\mathcal{L} = 3\mathcal{L}_{\min} = 3N(N-1)/2$ . I have performed calculations for  $\mathcal{L} = 3\mathcal{L}_{\min}$  and a number of other values of  $\mathcal{L}$  and confirm that for the density profile (15) this assumption is correct (it may however be wrong for other density profiles, see a comment in Section III B).

The number of basis many-body configurations  $N_{mbs}(N, \mathcal{L})$ , i.e., the size of the matrix  $\mathcal{H}_{ss'}$ , grows with  $N$  and  $\mathcal{L}$ , and at  $N = 7$  and  $\mathcal{L} = 3N(N-1)/2 = 63$  achieves  $N_{mbs}(N, \mathcal{L}) = N_{mbs}(7, 63) = 8033$ . This number is not extremely large, which allows one to calculate the matrix elements  $\mathcal{H}_{ss'}$  and to diagonalize the Hamiltonian matrix within reasonable computation time.

### III. EXACT SOLUTION

The physics of the considered system is determined by the interplay of attractive forces acting on electrons by the positively charged background, and the inter-electron forces repelling them from each other. Consider first a classical solution of this problem.

#### A. Classical Wigner crystal configurations

$N$  classical point charges in the attractive potential of the positive background may form two types of Wigner molecules (at small  $N$ ), Fig. 2: with a single shell, when all  $N$  particles are located on a ring of a finite radius  $R_s$ , Figs. 2(a)-2(e), and with two shells, when one particle is at the center of the positively charged disk, and  $N - 1$  particles are located on a ring around the center, Figs. 2(f)-2(h). I will denote these two configurations as  $(0, N)$  and  $(1, N - 1)$ , respectively. To understand which of the two possibilities is actually the case, one should calculate the total energy of the Wigner molecules in both situations.

The potential energy of the positively charged background disk is described by Eqs. (18)–(19) and is shown in Figure 1. In the single-shell configuration  $(0, N)$  the (dimensionless) complex coordinates of electrons can be written as, with  $R_s$  being the shell radius:

$$Z_j = R_s e^{i2\pi(j-1)/N}, \quad j = 1, 2, \dots, N. \quad (57)$$

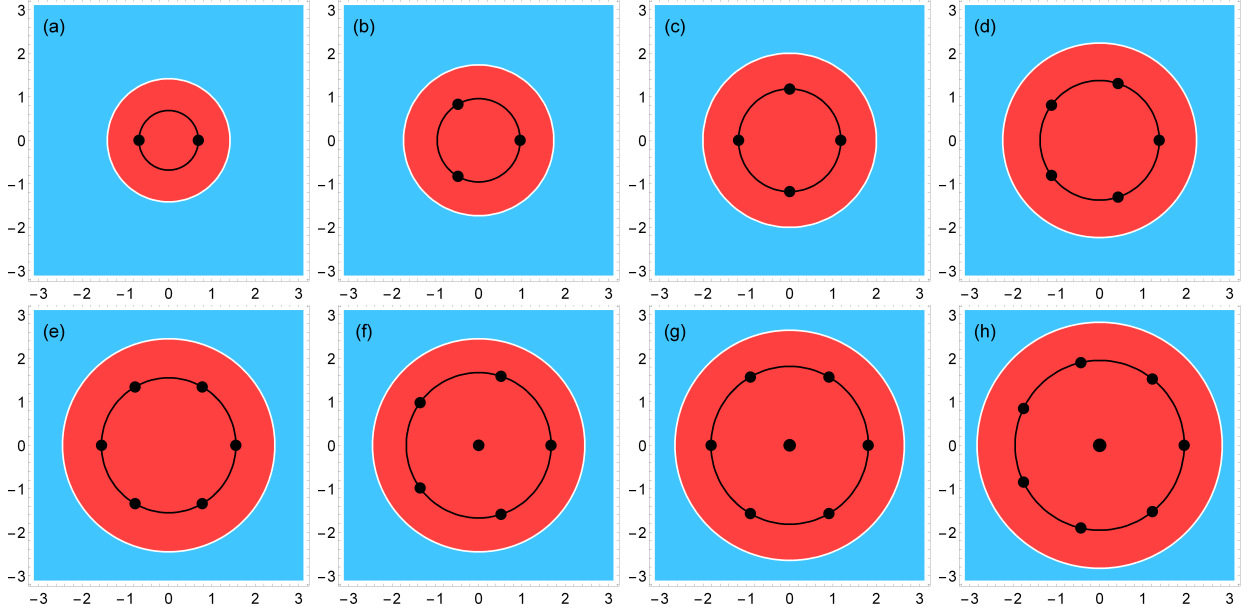


FIG. 2. Configurations of the Wigner crystal molecules in the field of the positive background with the density (15) for  $N = 2, \dots, 8$ . The white circle shows the boundary of the positively charged disk; the length unit is  $a_0$ . For  $N \leq 5$  the single-shell configurations (a)-(d) have a lower energy. For  $N \geq 7$  the two-shell configurations (g)-(h) have a lower energy. For  $N = 6$  the energies of the single-shell (e) and the two-shell (f) configurations are very close.

Then the total energy of the system is

$$E_{(0,N)}(R_s) = \sum_{j=1}^N U_N(|Z_j|) + \sum_{j=1}^{N-1} \sum_{k=j+1}^N \frac{1}{|Z_j - Z_k|} = N U_N(R_s) + \frac{1}{R_s} S_N, \quad (58)$$

where

$$S_N = \sum_{j=1}^{N-1} \sum_{k=j+1}^N \frac{1}{|1 - e^{i2\pi(k-j)/N}|}. \quad (59)$$

In the two-shell Wigner molecule  $(1, N-1)$ , the particle coordinates are

$$Z_j = R_s e^{i2\pi(j-1)/(N-1)}, \quad j = 1, 2, \dots, N-1, \quad Z_N = 0 \quad (60)$$

and the total energy has the form

$$E_{(1,N-1)}(R_s) = (N-1) U_N(R_s) + U_N(0) + \frac{1}{R_s} \left( S_{N-1} + (N-1) \right). \quad (61)$$

Minimizing the energies (58) and (61) with respect to  $R_s$  one can find the radii of the shells  $R_s(N)$  for both types of molecules and their total energies. The results of such calculations are shown in Table III. One sees that the energy of the  $(0, N)$  configuration is smaller than that of the  $(1, N-1)$  configuration, if  $N \leq 5$ . The opposite inequality,  $E_{(0,N)} > E_{(1,N-1)}$ , is valid at  $N \geq 7$ . If  $N = 6$ , the energies of both configurations are very close to each other: in the case of the density profile (15) the two-shell configuration has a slightly lower energy, with a difference of 0.051%. The  $N$ -dependencies of the Wigner molecule energies for both configurations are shown in Figure 3. The spatial distribution of the positive background density and the positions of charged point particles in the Wigner molecules are additionally illustrated in Figure 2.

Thus, the classical solution of the problem has the form of one-shell or two-shells Wigner molecules shown in Figure 2. It should therefore be expected that in the quantum-mechanical solution one will have, instead of point particles, broadened (e.g., Gaussian type) wave functions near each points, these wave function will overlap and their positions will be averaged over the angular coordinate. The electron density should therefore have the shape of a ring of radius  $R_s(N)$ , see Table III, with an additional density maximum at  $r = 0$ , if  $N \gtrsim 6$ . Now consider the exact quantum-mechanical solution of the problem.

TABLE III. Parameters of the Wigner molecules in one-shell  $(0, N)$  and two-shell  $(1, N - 1)$  configurations for the step-like density profile (15) and  $2 \leq N \leq 8$ .  $R$  is the radius of the positively charged background disk, and  $R_s(N)$  are the radii of the shells obtained by the minimization of the energies (58) and (61).  $E_{(0,N)}/N$  and  $E_{(1,N-1)}/N$  are the Wigner molecule energies per particle for two configurations. The lengths are in units  $a_0$ , the energies are in units  $e^2/a_0$ .

$N$	$R$	Configuration	$R_s(N)$	$E_{(0,N)}/N$	Configuration	$R_s(N)$	$E_{(1,N-1)}/N$
2	1.41421	(0,2)	0.684302	-2.289449			
3	1.73205	(0,3)	0.956542	-2.578969	(1,2)	1.196868	-2.460699
4	2.00000	(0,4)	1.178838	-2.813969	(1,3)	1.361107	-2.745380
5	2.23607	(0,5)	1.373422	-3.012388	(1,4)	1.518623	-2.983587
6	2.44949	(0,6)	1.549288	-3.184857	(1,5)	1.669034	-3.186483
7	2.64575	(0,7)	1.711287	-3.337907	(1,6)	1.812600	-3.362913
8	2.82843	(0,8)	1.862429	-3.475824	(1,7)	1.949843	-3.519063

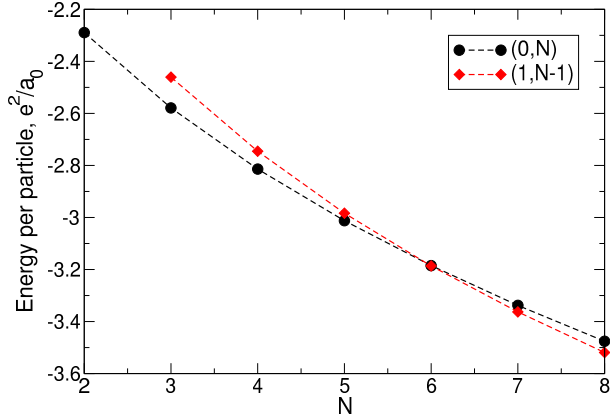


FIG. 3. The energy per particle of the Wigner crystal molecules in the  $N$  electron systems for  $(0, N)$  configurations at  $N = 2, \dots, 8$  and for  $(1, N - 1)$  configurations at  $N = 3, \dots, 8$ .

### B. Ground state energy and wave function

I have calculated a few lowest energy levels  $E_s^{3\mathcal{L}_{\min}}$ ,  $s = 1, 2, 3, \dots$ , for  $\nu = 1/3$  and  $\mathcal{L} = 3\mathcal{L}_{\min} = 3N(N - 1)/2$ , in the system with  $N = 2, 3, \dots, 7$  electrons. The third and fourth columns of Table IV show the energy of the lowest ( $s = 1$ ) and the next ( $s = 2$ ) energy levels; the second column gives the value of the corresponding total angular momentum  $\mathcal{L} = 3\mathcal{L}_{\min}$ . In addition, I have calculated the energies of a few neighboring angular momenta, and found that, for the total angular momentum  $\mathcal{L} = 3\mathcal{L}_{\min} - \delta\mathcal{L}$ , where

$$\delta\mathcal{L} = \begin{cases} N, & \text{if } N \leq 6, \\ N - 1, & \text{if } N = 7, \end{cases} \quad (62)$$

the lowest energy level  $E_1^{3\mathcal{L}_{\min} - \delta\mathcal{L}}$  lies between  $E_1^{3\mathcal{L}_{\min}}$  and  $E_2^{3\mathcal{L}_{\min}}$ ,

$$E_1^{3\mathcal{L}_{\min}} < E_1^{3\mathcal{L}_{\min} - \delta\mathcal{L}} < E_2^{3\mathcal{L}_{\min}}; \quad (63)$$

notice that the value of  $\delta\mathcal{L}$  coincides with the number of electrons on the outer shell in the Wigner molecule, see Figure 2. The fifth and sixth columns of Table IV show the angular momentum  $3\mathcal{L}_{\min} - \delta\mathcal{L}$  and the energy  $E_1^{3\mathcal{L}_{\min} - \delta\mathcal{L}}$ . Thus, the ground state energy of the system  $E_{\text{GS}}$  equals the lowest energy level of the state with  $\mathcal{L} = 3\mathcal{L}_{\min}$ , while the first excited state of the system  $E_{1\text{st}}$  equals the lowest energy level of the state with  $\mathcal{L} = 3\mathcal{L}_{\min} - \delta\mathcal{L}$ ,

$$E_{\text{GS}} = E_1^{3\mathcal{L}_{\min}}, \quad E_{1\text{st}} = E_1^{3\mathcal{L}_{\min} - \delta\mathcal{L}}. \quad (64)$$

The energy difference  $E_{1\text{st}} - E_{\text{GS}}$  between the first excited and the ground state (the seventh column in Table IV) is always smaller than  $0.1e^2/a_0$ . It mainly decreases as  $N$  grows. The case of  $N = 6$  particles is an exception related to the rearrangement of the shell structure from  $(0, N)$  into  $(1, N - 1)$  at  $N = 6$ , see Figures 2(e,f). Figure 4 shows

TABLE IV. Exact and Laughlin energies, as well as relevant angular momenta, of the lowest-energy states for different numbers of particles  $N$ . Second column: The total angular momentum  $3\mathcal{L}_{\min}$  corresponding to the true ground and Laughlin states. Third and fourth columns: The exact energies of the two lowest levels of the states with  $\mathcal{L} = 3\mathcal{L}_{\min}$ . Fifth and sixth columns: The total angular momentum  $3\mathcal{L}_{\min} - \delta\mathcal{L}$  and the lowest energy  $E_1^{3\mathcal{L}_{\min} - \delta\mathcal{L}}$  corresponding to the true first excited state. Seventh column: The energy difference  $E_{1\text{st}} - E_{\text{GS}}$  between the true first excited and the true ground state, Eq. (64). Eighth column: The exactly calculated energy of the Laughlin state. Ninth column: The energy difference  $E_{\text{RL}} - E_{\text{GS}}$  between the Laughlin state and the true ground state. All energies are in units  $e^2/a_0$ .

$N$	$3\mathcal{L}_{\min}$	$E_2^{3\mathcal{L}_{\min}}$	$E_1^{3\mathcal{L}_{\min}}$	$3\mathcal{L}_{\min} - \delta\mathcal{L}$	$E_1^{3\mathcal{L}_{\min} - \delta\mathcal{L}}$	$E_{1\text{st}} - E_{\text{GS}}$	$E_{\text{RL}}$	$E_{\text{RL}} - E_{\text{GS}}$
2	3	-1.872042	-1.447705	1	-1.773044	0.098998	-1.871568	0.000474
3	9	-2.852911	-2.479623	6	-2.811722	0.041189	-2.840219	0.012692
4	18	-3.837655	-3.534888	14	-3.813058	0.024597	-3.809984	0.027671
5	30	-4.810806	-4.610344	25	-4.786288	0.024518	-4.779627	0.031179
6	45	-5.783597	-5.645735	39	-5.741990	0.041606	-5.754097	0.029500
7	63	-6.775065	-6.626187	57	-6.767761	0.007304	-6.732099	0.042965

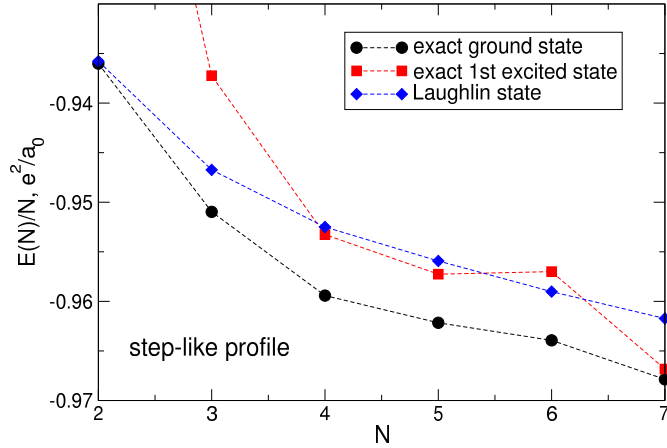


FIG. 4. The energy per particle of the exact ground (black circles) and the first excited (red squares) states, Eq. (64), as well as of the Laughlin state (5) at  $\nu = 1/3$  as a function of the number of particles  $N$ . The energies are in units  $e^2/a_0$ .

the energies (per particle) of the ground and the first excited states, Eq. (64), as a function of the electron number  $N$  (black circles and red squares, respectively).

The expansion coefficients  $A_s^{\text{GS}}$  of the ground state many-body wave functions  $|\Psi_{\text{GS}}\rangle$  over the basis states  $|\Psi_s\rangle$ , see Eq. (55), are shown in Tables V and VI for two and three particles. The largest contribution to the ground state wave function for  $N = 2$  and 3 is given by the states  $|1, 2\rangle$  and  $|2, 3, 4\rangle$ , respectively, i.e., the states in which the individual angular momenta of particles  $L_j^{(s)}$  are the closest to the average value  $\mathcal{L}/N$ . The vectors  $A_s^{\text{GS}}$  for  $N \geq 4$  particles can be found in Supplementary Materials, see Appendix C.

TABLE V. The expansion coefficients  $A_s^{\text{GS}}$  for the exact ground state of  $N = 2$  particles.

$s$	state	$A_s^{\text{GS}}$
1	$ 0, 3\rangle$	-0.47078
2	$ 1, 2\rangle$	0.88225

TABLE VI. The expansion coefficients  $A_s^{\text{GS}}$  for the exact ground state of  $N = 3$  particles.

$s$	state	$A_s^{\text{GS}}$
1	$ 0, 1, 8\rangle$	0.01613
2	$ 0, 2, 7\rangle$	-0.03971
3	$ 0, 3, 6\rangle$	-0.08983
4	$ 0, 4, 5\rangle$	0.32071
5	$ 1, 2, 6\rangle$	0.29234
6	$ 1, 3, 5\rangle$	-0.44922
7	$ 2, 3, 4\rangle$	0.77458

### C. Density of electrons in the ground state

The density of electrons in the exact ground states in systems with different  $N$  can be calculated using the matrix elements (33) and the expansion coefficients of the exact ground state wave function  $A_s^{\text{GS}}$ ,

$$n_e^{\text{GS}}(r) = \sum_{s=1}^{N_{\text{mbs}}} (A_s^{\text{GS}})^2 \sum_{j=1}^N |\psi_{L_j^{(s)}}(\mathbf{r})|^2. \quad (65)$$

The results of calculations are shown in Figure 5(a) for  $N = 2, \dots, 7$ . The electron density calculated by quantum mechanics is in complete agreement with the expectations arising from the classical considerations in Section III A. When  $N$  grows from 2 to 4, the density curves have maxima at the points which are very close to the radii of the classical Wigner molecules for these  $N$ , and the densities in the disk center  $n_e(r = 0)$  decrease, since as  $N$  increases, the electrons repel stronger from the disk center. Starting from  $N = 5$  the probability of finding one electron in the disk center starts to grow. At  $N = 5$ , the density at  $r = 0$  increases, and the maximum of the curve shifts slightly beyond the position of the classical Wigner molecule shell, since this central electron pushes the other electrons towards the edge of the disk. At  $N = 6$ , a local maximum at  $r = 0$  appears. At  $N = 7$  a giant maximum arises in the disk center, with the value of  $n_e(r = 0)$ , larger than the  $n_e$ -maximum at a finite  $r \simeq R_s$ .

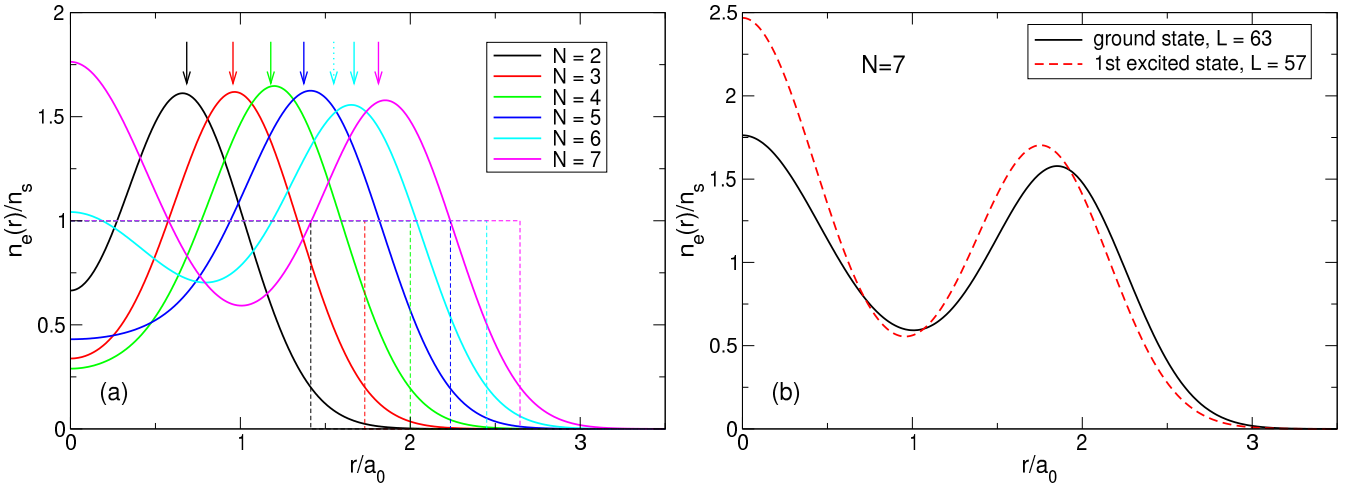


FIG. 5. (a) The density of electrons in the exact ground state (thick solid curves), together with the density of the positive background (thin dashed curves) for  $N = 2 \dots 7$  for the step-like background density profile (15). Arrows above the curves show the radii of the outer shells  $R_s(N)$  of the Wigner molecules, see Table III; for  $N = 6$  the shell radii of both  $(0, N)$  (dashed arrow) and  $(1, N - 1)$  (solid arrow) configurations are shown. (b) The density of electrons in the exact ground state ( $\mathcal{L} = 63$ ) and the first excited state ( $\mathcal{L} = 57$ ) for  $N = 7$ .

Figure 5(b) shows the density of electrons in the exact ground state ( $\mathcal{L} = 63$ ) and in the first excited state ( $\mathcal{L} = 57$ ) for seven particles. It can be seen that the distribution of electrons in the first excited state also resembles a Wigner molecule, but with somewhat different parameters: in the excited state, the probability of finding an electron in the disk center is higher than in the ground state, and the radius of the outer shell of the electron ring is slightly smaller.

The exact quantum-mechanical solution thus clearly shows that the ground state of a few (up to  $N = 7$ ) two-dimensional electrons at the Landau level filling factor  $\nu = 1/3$  has the form resembling a floating (or sliding) Wigner crystal molecule [30–34]. This agrees with the intuitive understanding of the physics of Coulomb-interacting particles.

#### D. Pair correlation function in the ground state

The pair correlation function in the ground state can be calculated using the formula

$$P_{\text{GS}}(\mathbf{r}, \mathbf{r}') = \sum_{s=1}^{N_{\text{mbs}}} A_s^{\text{GS}} \sum_{s'=1}^{N_{\text{mbs}}} A_{s'}^{\text{GS}} \langle \Psi_s | \hat{P}(\mathbf{r}, \mathbf{r}') | \Psi_{s'} \rangle, \quad (66)$$

with the matrix elements determined by Eqs. (52)–(53). Examples of the calculated function  $P_{\text{GS}}(\mathbf{r}, \mathbf{r}')$  are shown in Figure 6. Here, the colored distribution shows the probability to find an electron at a point  $\mathbf{r}$ , under the condition that another electron is fixed at the point  $\mathbf{r}'$  shown by small black circles on the panels. The panels (a), (b), and (c) illustrate the cases when the points  $\mathbf{r}'$  are outside the disk center at the distance corresponding to the maxima of the electron density, see Figure 5. Figure 6(a) illustrates the case of  $N = 3$  particles. One sees a triangular structure which resembles the classical Wigner molecule configuration shown in Figure 2(b). Starting from  $N = 4$ , crystalline electron-electron correlations are significantly weakened: they are still weakly seen in Figure 6(b) corresponding to  $N = 4$ , but becomes invisible at larger  $N$ , see Figure 6(c) for  $N = 6$ , where only one maximum is seen opposite to the point  $\mathbf{r}'$ . This is a consequence of the significant overlap of single-particle wave functions and of the averaging over the angular coordinate in the ground state which looks similarly to a sliding Wigner-crystal molecule.

Figure 6(d) shows the pair correlation function for the case  $N = 7$  and  $\mathbf{r}' = \mathbf{0}$ . Now the function  $P_{\text{GS}}(\mathbf{r}, \mathbf{0})$  is circularly symmetric and has a maximum at  $r \approx 1.16a_0$ . The behavior of  $P(\mathbf{r}, \mathbf{0})$  at small  $r$  is quadratic,  $P_{\text{GS}}(\mathbf{r}, \mathbf{0}) \propto r^2$  at  $r \rightarrow 0$ .

### IV. MAXIMUM DENSITY DROPLET STATE, $\nu = 1$

Using the mathematical apparatus developed in Section II, one can now calculate properties of the states (5) for few-electron systems and compare them with those of the exact ground state. But before proceeding to the discussion of the case  $m = 3$  ( $\nu = 1/3$ ), it will be useful to briefly overview physical properties of the MDD configuration [7] which is a special case of the function (5) at  $m = 1$ .

#### A. Wave function

The MDD configuration

$$\Psi_{\text{mdd}} = |0, 1, 2, \dots, N-1\rangle = \frac{1}{\sqrt{N!}} \det \begin{vmatrix} \psi_0(\mathbf{r}_1) & \psi_0(\mathbf{r}_2) & \dots & \psi_0(\mathbf{r}_N) \\ \psi_1(\mathbf{r}_1) & \psi_1(\mathbf{r}_2) & \dots & \psi_1(\mathbf{r}_N) \\ \dots & \dots & \dots & \dots \\ \psi_{N-1}(\mathbf{r}_1) & \psi_{N-1}(\mathbf{r}_2) & \dots & \psi_{N-1}(\mathbf{r}_N) \end{vmatrix}, \quad (67)$$

describes the ground state of the system at  $\nu = 1$ , if the influence of higher Landau levels is neglected, Ref. [7]. In this configuration,  $N$  electrons occupy the lowest Landau level single-particle states with the smallest possible individual angular momenta from  $L = 0$  up to  $L = N - 1$ . Since  $\psi_L(\mathbf{r})$  is proportional to  $z^L$ , the matrix in (67) has the form of the Vandermonde matrix, and its determinant can be presented in the form (5) with  $m = 1$ . The total angular momentum in the MDD state is  $\mathcal{L} = \mathcal{L}_{\text{min}} = N(N-1)/2$ , Eq. (29). The number of many-body configurations for a given  $N$  and  $\mathcal{L} = \mathcal{L}_{\text{min}}$  equals one,  $N_{\text{mbs}}(N, \mathcal{L}_{\text{min}}) = 1$ .

#### B. Energy of an $N$ -particle system

The energy of the MDD state

$$E_{\text{mdd}}(N) = \langle \Psi_{\text{mdd}} | \hat{V}_{bb} + \hat{V}_{be} + \hat{V}_{ee} | \Psi_{\text{mdd}} \rangle \quad (68)$$

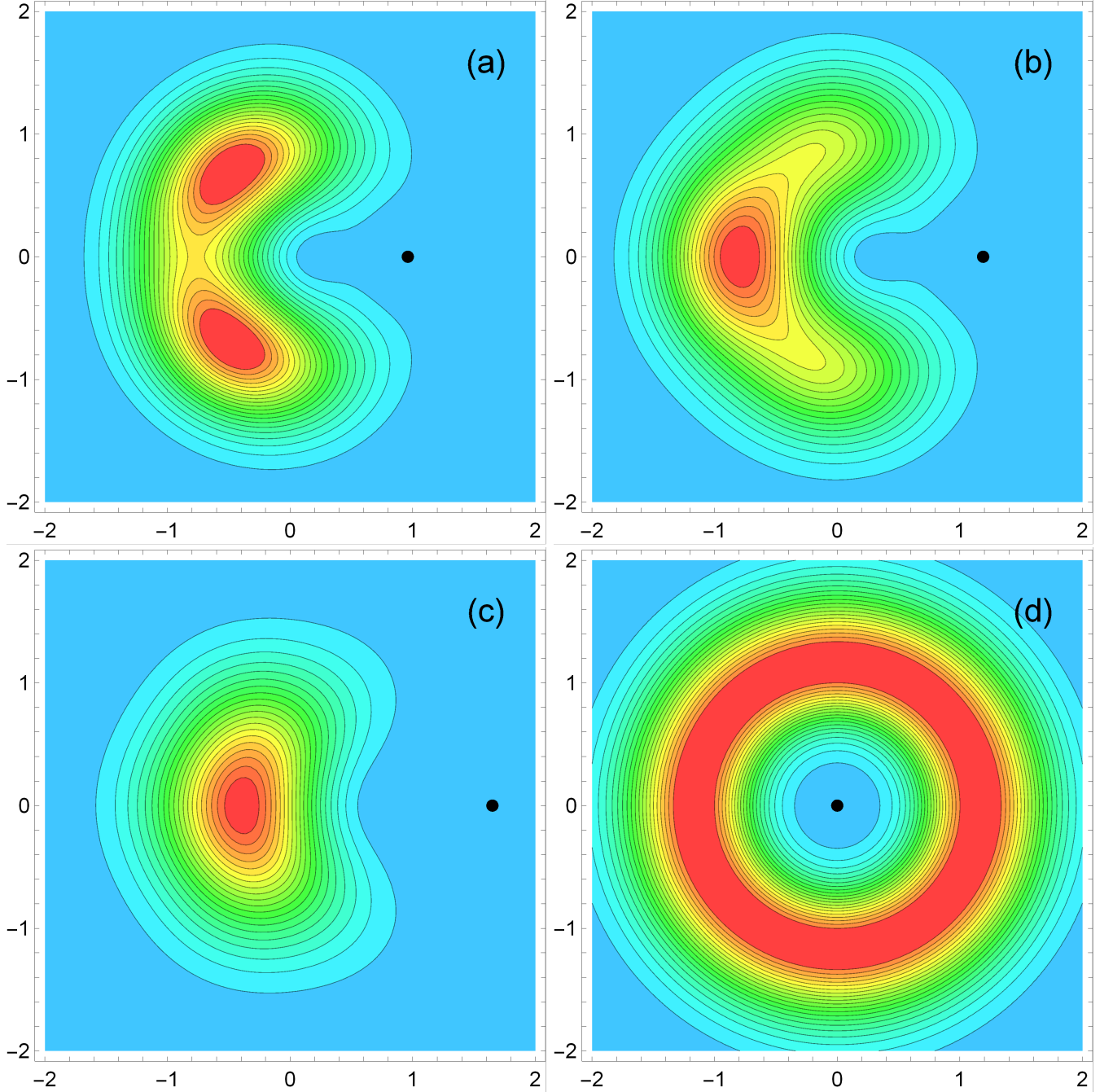


FIG. 6. The pair correlation function  $P_{\text{GS}}(\mathbf{r}, \mathbf{r}')$  in the ground state, as a function of  $x/a_0$  and  $y/a_0$ , for different  $N$  and different coordinates  $\mathbf{r}'$ : (a)  $N = 3$  and  $\mathbf{r}'/a_0 = (0.96, 0)$ , (b)  $N = 4$  and  $\mathbf{r}'/a_0 = (1.19, 0)$ , (c)  $N = 6$  and  $\mathbf{r}'/a_0 = (1.65, 0)$ , and (d)  $N = 7$  and  $\mathbf{r}'/a_0 = (0, 0)$ . The positions of the  $\mathbf{r}'$  points are shown by small black circles; in (a), (b), and (c) they correspond to the maxima of the electron density, see Figure 5.

can be calculated using the Coulomb matrix elements found in Section II E. The background-background interaction energy in this formula is given by Eq. (36), calculation of the background-electron interaction energy in the MDD case gives

$$\langle \Psi_{\text{mdd}} | \hat{V}_{be} | \Psi_{\text{mdd}} \rangle = -N \frac{e^2}{a_0} 2 \frac{\Gamma(N + \frac{1}{2})}{\Gamma(N)} {}_2F_2 \left( -\frac{1}{2}, \frac{1}{2}; 2, \frac{1}{2} - N; -N \right), \quad (69)$$

see Appendix A 2, and the electron-electron (Hartree minus Fock) interaction energy is

$$\langle \Psi_{\text{mdd}} | \hat{V}_{ee} | \Psi_{\text{mdd}} \rangle = \frac{e^2}{a_0} \sqrt{\frac{\pi}{2}} \sum_{L=0}^{N-2} \sum_{L'=L+1}^{N-1} [\mathcal{K}(L, L', 0) - \mathcal{K}(L, L, L' - L)], \quad (70)$$

The energy (68) (per particle) calculated for  $N$  up to  $N = 100$  is shown in Figure 7 by the black curves and symbols, as a function of  $N$  in Figure 7(a), and as a function of  $N^{-1/2}$  in Figure 7(b).

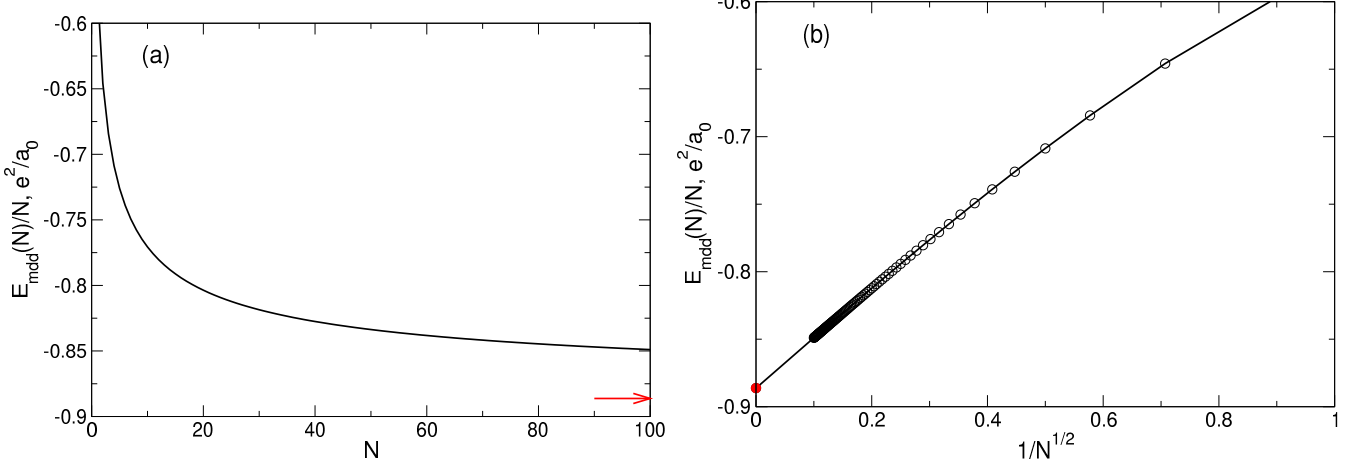


FIG. 7. The energy per particle of the MDD state (67), measured in units  $e^2/a_0$ , (a) as a function of the number of electrons  $N$  and (b) as a function of  $1/\sqrt{N}$ . The red arrow in (a) and red point in (b) show the asymptotic value (78), reported in Ref. [6].

### C. Electron density

The density of electrons in the MDD state (67), according to (33), is

$$n_e^{\text{mdd}}(\mathbf{r}) = \sum_{L=0}^{N-1} |\psi_L(\mathbf{r})|^2 = \frac{1}{\pi \lambda^2} e^{-r^2/\lambda^2} \sum_{L=0}^{N-1} \frac{(r/\lambda)^{2L}}{L!} = n_s Q(N, r^2/\lambda^2), \quad (71)$$

where

$$Q(N, x) = \frac{\Gamma(N, x)}{\Gamma(N)} \quad (72)$$

is the regularized incomplete Gamma function. The density  $n_e^{\text{mdd}}(r)$  is constant and equals  $n_s$  up to  $r \simeq R - \lambda = R - a_0$ , Figure 8. In the limit  $N \rightarrow \infty$  the density  $n_e^{\text{mdd}}(r)$  becomes homogeneous in the whole 2D space. The state (67) thus describes an ideally uniform liquid, which is a consequence of the fact that, being an eigenfunction of the kinetic energy operator, the function (67) does not satisfy the many-body Schrödinger equation (54)–(21), so that the Coulomb interaction is completely ignored in this state.

### D. Pair correlation function

The pair correlation function of the MDD configuration can be found by calculating the average value of the operator (51) with the wave function (67). It can be presented in the form

$$P(\mathbf{r}, \mathbf{r}') = n_e(\mathbf{r}) n_e(\mathbf{r}') + \delta P(\mathbf{r}, \mathbf{r}'), \quad (73)$$

where

$$\delta P_{\text{mdd}}(\mathbf{r}, \mathbf{r}') = -n_s^2 e^{-|z-z'|^2} Q(N, z z'^*) Q(N, z^* z'), \quad (74)$$

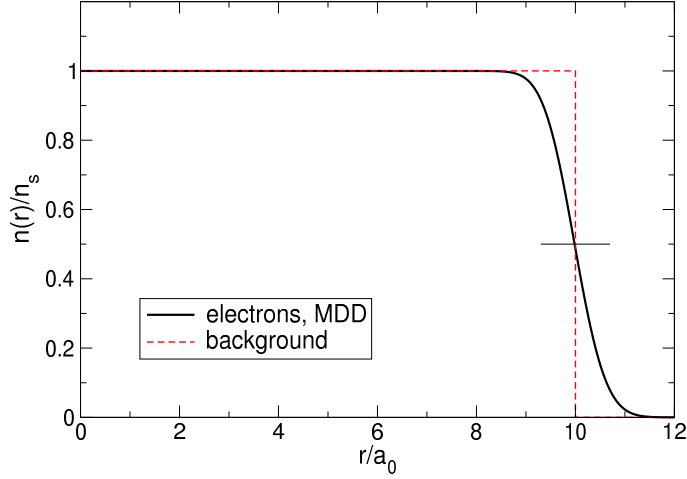


FIG. 8. The density of electrons in the MDD state at  $\nu = 1$  (black solid curve) and the density of the positive background  $n_b(r)$  (red dashed curve) for  $N = 100$ . The density is plotted as a function of  $r/a_0$  or  $r/\lambda$  (at  $\nu = 1$   $\lambda = a_0$ ).

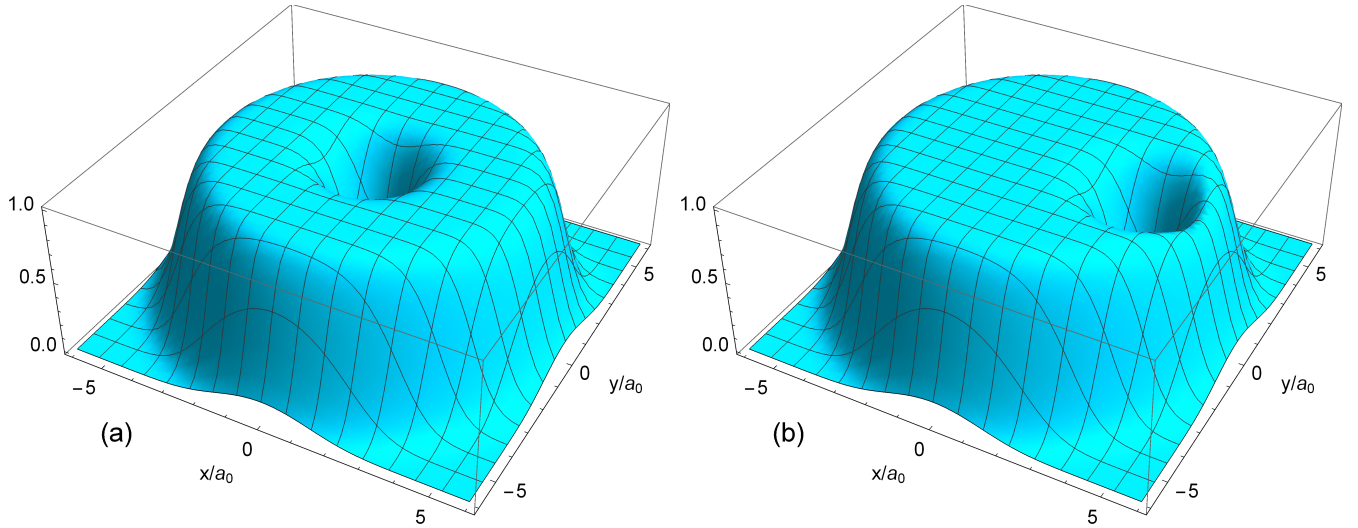


FIG. 9. The pair correlation function of the MDD state (67), as a function of  $\mathbf{r}/a_0$ , at  $N = 30$  and (a)  $\mathbf{r}'/a_0 = (0, 0)$  and (b)  $\mathbf{r}'/a_0 = (3, 0)$ .

and  $z = (x - iy)/\lambda$ . The dependence of  $P_{\text{mdd}}(\mathbf{r}, \mathbf{r}')$  on  $x/a_0$  and  $y/a_0$  at  $\mathbf{r}'/a_0 = (0, 0)$  and  $\mathbf{r}'/a_0 = (3, 0)$  for  $N = 30$  particles is shown in Fig. 9. The pair correlation function tends to unity when  $|\mathbf{r} - \mathbf{r}'|/a_0 \gg 1$  and both points,  $\mathbf{r}$  and  $\mathbf{r}'$ , are far from the system boundaries. In the limit  $|\mathbf{r} - \mathbf{r}'| \rightarrow 0$  the function  $P_{\text{mdd}}(\mathbf{r}, \mathbf{r}')$  tends to zero as  $|\mathbf{r} - \mathbf{r}'|^2$ , due to the exchange “interaction”.

### E. Thermodynamic limit

If  $\Psi$  is a many-body wave function of an  $N$ -particle system, the average value of the energy in this state  $E(N) = \langle \Psi | \hat{\mathcal{H}} | \Psi \rangle = \langle \Psi | \hat{V}_C | \Psi \rangle$  can be presented in the form (I omit the kinetic energy contribution  $N\hbar\omega_c/2$ )

$$E(N) = \langle \Psi | \hat{V}_C | \Psi \rangle = \frac{e^2}{2} \int \frac{d\mathbf{r} d\mathbf{r}'}{|\mathbf{r} - \mathbf{r}'|} \delta n(\mathbf{r}) \delta n(\mathbf{r}') + \frac{e^2}{2} \int \frac{d\mathbf{r} d\mathbf{r}'}{|\mathbf{r} - \mathbf{r}'|} \delta P(\mathbf{r}, \mathbf{r}'), \quad (75)$$

where  $\delta n(\mathbf{r}) = n_e(\mathbf{r}) - n_b(\mathbf{r})$ , and  $\delta P(\mathbf{r}, \mathbf{r}')$  is defined in Eq. (73). The first term in (75) is the Hartree energy, which vanishes if the electron and positive background densities are identical. This condition is satisfied at  $\nu = 1$  in the MDD state in the limit  $N \rightarrow \infty$ , when the density of electrons  $n_e^{\text{mdd}}(r)$  becomes ideally uniform in the whole 2D

space,  $n_e^{\text{mdd}}(r) \rightarrow n_s$ . The regularized incomplete Gamma function  $Q(N, x)$  tends to unity at  $N \rightarrow \infty$ , and the pair correlation function (74) becomes a function of only the inter-particle distance  $|\mathbf{r} - \mathbf{r}'|$ ,

$$\delta P_{\text{mdd}}(\mathbf{r} - \mathbf{r}') = -n_s^2 e^{-|\mathbf{r} - \mathbf{r}'|^2/a_0^2}. \quad (76)$$

For the MDD energy one then gets from (75)

$$E_{\text{mdd}}(N) \approx \frac{e^2}{2} \int d\mathbf{r} \int \frac{d\mathbf{r}'}{|\mathbf{r} - \mathbf{r}'|} \delta P_{\text{mdd}}(|\mathbf{r} - \mathbf{r}'|) \approx \frac{e^2}{2} \pi R^2 \int \frac{d\mathbf{r}'}{|\mathbf{r}'|} \delta P_{\text{mdd}}(|\mathbf{r}'|). \quad (77)$$

Since  $\pi R^2 n_s = N$  this gives the energy per particle in the thermodynamic limit  $N \rightarrow \infty$

$$\frac{E_{\text{mdd}}(N)}{N} = \frac{\pi e^2}{n_s} \int_0^\infty dr \delta P_{\text{mdd}}(r) = -\frac{e^2}{a_0} \frac{\sqrt{\pi}}{2}. \quad (78)$$

This formula was reported for  $\nu = 1$  in Ref. [6]. The asymptotic value (78) is shown by the red arrow and red point in Figures 7(a) and 7(b). Notice that the formulas (77) and (78) are valid only if the density of electrons is uniform in the whole 2D space – only in this case the Hartree energy in (75) vanishes and the pair correlation function  $P_{\text{mdd}}(\mathbf{r}, \mathbf{r}')$  becomes a function of  $|\mathbf{r} - \mathbf{r}'|$ .

## V. LAUGHLIN WAVE FUNCTION AT $\nu = 1/3$

### A. General remarks

Laughlin suggested, by analogy with (67), that the ground state of the system at  $\nu = 1/3$  is determined by the function (5) with  $m = 3$ ,

$$\Psi_{\text{RL}} \propto \left( \prod_{1 \leq j < k \leq N} (z_j - z_k)^3 \right) \exp \left( -\frac{1}{2} \sum_{j=1}^N |z_j|^2 \right), \quad (79)$$

and that this function describes a “liquid” state with a uniform electron density. In order to calculate the energy, electron density, and other physical properties of the system in the state (79) I proceed as follows.

The function (79) is the eigenfunction of the angular momentum operator with the eigenvalue

$$\mathcal{L} = m \frac{N(N-1)}{2} = 3 \frac{N(N-1)}{2}. \quad (80)$$

For any given  $N$  and  $\mathcal{L}$  I determine  $N_{\text{mbs}}$  many-body states, formed from the lowest Landau level single-particle functions (12), and expand the Laughlin wave function in these basis states,

$$\Psi_{\text{RL}} = \sum_{s=1}^{N_{\text{mbs}}} A_s^{\text{RL}} \Psi_s. \quad (81)$$

The coefficients  $A_s^{\text{RL}}$  here are real numbers, and the function (81) is assumed to be normalized, i.e.,  $\sum_{s=1}^{N_{\text{mbs}}} (A_s^{\text{RL}})^2 = 1$ . After the coefficients  $A_s^{\text{RL}}$  are found, any physical quantity  $F$  can be calculated as the average

$$F = \langle \Psi_{\text{RL}} | \hat{F} | \Psi_{\text{RL}} \rangle = \sum_{s=1}^{N_{\text{mbs}}} \sum_{s'=1}^{N_{\text{mbs}}} A_s^{\text{RL}} A_{s'}^{\text{RL}} \langle \Psi_s | \hat{F} | \Psi_{s'} \rangle, \quad (82)$$

where the matrix elements  $\langle \Psi_s | \hat{F} | \Psi_{s'} \rangle$  are found in Section II E for commonly used operators. How to calculate the coefficients  $A_s^{\text{RL}}$ ?

### B. Expansion coefficients of the Laughlin function

The coefficients  $A_s^{\text{RL}}$  in (81) can be found as follows. First, using the binomial expansion of the polynomial factors in the Laughlin function (79), I obtain integer binomial coefficients  $C_s$ , as in the following example for two particles:

$$(z_1 - z_2)^3 = z_1^3 - 3z_1^2z_2 + 3z_1z_2^2 - z_2^3 = (-1) \det \begin{vmatrix} z_1^0 & z_2^0 \\ z_1^3 & z_2^3 \end{vmatrix} + 3 \det \begin{vmatrix} z_1^1 & z_2^1 \\ z_1^2 & z_2^2 \end{vmatrix}; \quad (83)$$

I denote the coefficients  $C_s$  as

$$C_{|0,3\rangle} = -1 \quad \text{and} \quad C_{|1,2\rangle} = 3. \quad (84)$$

The determinants in (83) are proportional to the basis functions  $|0, 3\rangle$  and  $|1, 2\rangle$ . For example

$$|0, 3\rangle = \frac{1}{\sqrt{2!}} \det \begin{vmatrix} \psi_0(\mathbf{r}_1) & \psi_0(\mathbf{r}_2) \\ \psi_3(\mathbf{r}_1) & \psi_3(\mathbf{r}_2) \end{vmatrix} = \frac{1}{\sqrt{2!}} \det \begin{vmatrix} z_1^0 & z_2^0 \\ z_1^3 & z_2^3 \end{vmatrix} \frac{e^{-(|z_1|^2 + |z_2|^2)/2}}{\pi \lambda^2 \sqrt{0!3!}}, \quad (85)$$

so that one gets

$$\det \begin{vmatrix} z_1^0 & z_2^0 \\ z_1^3 & z_2^3 \end{vmatrix} \propto \sqrt{0!3!} |0, 3\rangle. \quad (86)$$

Then the expansion of the Laughlin function for two particles takes the form

$$(z_1 - z_2)^3 e^{-(|z_1|^2 + |z_2|^2)/2} \propto D_{|0,3\rangle} |0, 3\rangle + D_{|1,2\rangle} |1, 2\rangle, \quad (87)$$

where

$$D_{|L_1, L_2\rangle} = \sqrt{L_1! L_2!} C_{|L_1, L_2\rangle}. \quad (88)$$

Thus, in order to calculate (for any  $N$ ) the real coefficients  $A_s^{\text{RL}}$  in the expansion (81) one needs to find, first, the integers binomial coefficients  $C_s = C_{|L_1, L_2, \dots, L_N\rangle}$  in the expansions of the polynomial factors in (79), then calculate the  $D_s$  factors according to the formula

$$D_{|L_1, L_2, \dots, L_N\rangle} = \sqrt{L_1! L_2! \dots L_N!} C_{|L_1, L_2, \dots, L_N\rangle}, \quad (89)$$

and finally determine the real coefficients  $A_s^{\text{RL}}$  by using the normalization condition

$$A_s^{\text{RL}} = \frac{D_s}{\sqrt{\sum_{p=1}^{N_{\text{mbs}}} D_p^2}}. \quad (90)$$

Now I apply the described algorithm to the Laughlin wave function for a few values of the particle number  $N$ .

#### 1. Two particles

If  $N = 2$ , then the angular momentum (80) at  $\nu = 1/3$  equals  $\mathcal{L} = 3$ . The number of many-body states in this case is  $N_{\text{mbs}} = 2$ , and they are  $|0, 3\rangle$  and  $|1, 2\rangle$ , see Table I. Expanding the factor  $(z_1 - z_2)^3$  as in (83) I get the coefficients  $C_s$ , Eq. (84),  $D_s$ ,  $A_s^{\text{RL}}$ , and  $(A_s^{\text{RL}})^2$ . The results are shown in Table VII.

TABLE VII. Many-body configurations for  $N = 2$  and  $\mathcal{L} = 3$ , with the expansion coefficients  $C_s$ ,  $A_s^{\text{RL}}$ , and  $(A_s^{\text{RL}})^2$ . The coefficients  $D_s$  can be found using Eq. (89).

No.	Configuration	$C_s$	$A_s^{\text{RL}}$	$(A_s^{\text{RL}})^2$
1	$ 0, 3\rangle$	-1	-0.5	0.25
2	$ 1, 2\rangle$	3	0.86603	0.75

## 2. Three particles

If  $N = 3$ , then the angular momentum (80) equals  $\mathcal{L} = 9$ . Now one has  $N_{mbs} = 7$  many-body states, see Table II. Using again the binomial expansion

$$(z_1 - z_2)^3(z_1 - z_3)^3(z_2 - z_3)^3 \propto -\Delta_{|0,3,6\rangle} + 3\Delta_{|0,4,5\rangle} + 3\Delta_{|1,2,6\rangle} - 6\Delta_{|1,3,5\rangle} + 15\Delta_{|2,3,4\rangle}, \quad (91)$$

where

$$\Delta_{|j,k,l\rangle} = \det \begin{vmatrix} z_1^j & z_2^j & z_3^j \\ z_1^k & z_2^k & z_3^k \\ z_1^l & z_2^l & z_3^l \end{vmatrix}, \quad (92)$$

I get the coefficients  $C_s$ ,  $A_s^{\text{RL}}$ , and  $(A_s^{\text{RL}})^2$  shown in Table VIII. Not all possible basis functions  $\Psi_s$  are represented in the Laughlin function (79). Two configurations,  $|0, 1, 8\rangle$  and  $|0, 2, 7\rangle$ , have zero weights in  $\Psi_{\text{RL}}$ .

TABLE VIII. Many-body configurations for  $N = 3$  and  $\mathcal{L} = 9$ , with the expansion coefficients  $C_s$ ,  $A_s^{\text{RL}}$ , and  $(A_s^{\text{RL}})^2$ . The coefficients  $D_s$  can be found using Eq. (89).

No.	Configuration	$C_s$	$A_s^{\text{RL}}$	$(A_s^{\text{RL}})^2$
1	$ 0, 1, 8\rangle$	0	0.0	0.0
2	$ 0, 2, 7\rangle$	0	0.0	0.0
3	$ 0, 3, 6\rangle$	-1	-0.17961	0.03226
4	$ 0, 4, 5\rangle$	3	0.43994	0.19355
5	$ 1, 2, 6\rangle$	3	0.31109	0.09677
6	$ 1, 3, 5\rangle$	-6	-0.43994	0.19355
7	$ 2, 3, 4\rangle$	15	0.69561	0.48387

## 3. Four particles

If  $N = 4$ , then the total angular momentum (80) equals  $\mathcal{L} = 18$ , and the number of many-body states is  $N_{mbs} = 34$ . Applying the binomial expansion procedure I calculate the numbers  $C_s$ . Only 16 of them are nonzero; these states, the corresponding integer binomial coefficients  $C_s$ , as well as the numbers  $A_s^{\text{RL}}$  and  $(A_s^{\text{RL}})^2$ , are shown in Table IX. Other 18 states, namely the states

$$\begin{aligned} &|0, 1, 2, 15\rangle, |0, 1, 3, 14\rangle, |0, 1, 4, 13\rangle, |0, 1, 5, 12\rangle, |0, 1, 6, 11\rangle, |0, 1, 7, 10\rangle, |0, 1, 8, 9\rangle, \\ &|0, 2, 3, 13\rangle, |0, 2, 4, 12\rangle, |0, 2, 5, 11\rangle, |0, 2, 6, 10\rangle, |0, 2, 7, 9\rangle, \\ &|0, 3, 4, 11\rangle, |0, 3, 5, 10\rangle, \\ &|1, 2, 3, 12\rangle, |1, 2, 4, 11\rangle, |1, 2, 5, 10\rangle, \\ &|1, 3, 4, 10\rangle \end{aligned}$$

have zero weights  $C_s = 0$  in the Laughlin wave function.

## 4. Five to eight particles

The cases of  $N = 5, \dots, 8$  particles can be analyzed similarly. The full tables with all many-body configurations and their weights are very large and not shown here; they can be found in Supplementary Materials, see Appendix C. Here, I give only a brief overview of some key features of the Laughlin function expansions that are useful for the subsequent analysis of the problem.

The number of many-body configurations which are *not* used in the Laughlin wave function dramatically grows with the number of particles  $N$ . Table X shows the total number of many-body configurations for given  $N$  and  $\mathcal{L}$ ,  $N_{mbs}(N, \mathcal{L})$ , the number of states which do not contribute to the Laughlin wave function  $N_{mbs}^{=0}$ , the number of states which give a nonzero contribution to  $\Psi_{\text{RL}}$ ,  $N_{mbs}^{\neq 0}$ , and the percentage of many-body configuration *not contributing* to

TABLE IX. Many-body configurations for  $N = 4$  and  $\mathcal{L} = 18$ , with the expansion coefficients  $C_s$ ,  $A_s^{\text{RL}}$ , and  $(A_s^{\text{RL}})^2$ . The coefficients  $D_s$  can be found using Eq. (89).

No.	Configuration	$C_s$	$A_s^{\text{RL}}$	$(A_s^{\text{RL}})^2$
15	$ 0, 3, 6, 9\rangle$	1	0.05322	0.00283
16	$ 0, 3, 7, 8\rangle$	-3	-0.14082	0.01983
17	$ 0, 4, 5, 9\rangle$	-3	-0.13037	0.01700
18	$ 0, 4, 6, 8\rangle$	6	0.21290	0.04533
19	$ 0, 5, 6, 7\rangle$	-15	-0.42078	0.17705
23	$ 1, 2, 6, 9\rangle$	-3	-0.09219	0.00850
24	$ 1, 2, 7, 8\rangle$	9	0.24391	0.05949
26	$ 1, 3, 5, 9\rangle$	6	0.13037	0.01700
27	$ 1, 3, 6, 8\rangle$	-12	-0.21290	0.04533
28	$ 1, 4, 5, 8\rangle$	-9	-0.13037	0.01700
29	$ 1, 4, 6, 7\rangle$	27	0.33872	0.11473
30	$ 2, 3, 4, 9\rangle$	-15	-0.20614	0.04249
31	$ 2, 3, 5, 8\rangle$	27	0.27656	0.07649
32	$ 2, 3, 6, 7\rangle$	-6	-0.05322	0.00283
33	$ 2, 4, 5, 7\rangle$	-45	-0.32593	0.10623
34	$ 3, 4, 5, 6\rangle$	105	0.49787	0.24788

the Laughlin function (79) (denoted as “% zero” in the Table X). One sees that, while for  $N = 3$  “only” 28.57% of all possible many-body configurations are not used in the Laughlin wave function, at  $N = 8$  this number increases up to 90.54%.

TABLE X. The total number of many-body states  $N_{\text{mbs}}$ , the number of states contributing ( $N_{\text{mbs}}^{>0}$ ) and not contributing ( $N_{\text{mbs}}^{=0}$ ) to the Laughlin function, as well as the percentage of non-contributing many-body configurations ('% zero').  $N$  is the number of particles and  $\mathcal{L}$  is the total angular momentum (80) corresponding to  $\nu = 1/3$  and  $m = 3$  in Eq. (5).

$N$	$\mathcal{L}$	$N_{\text{mbs}}$	$N_{\text{mbs}}^{=0}$	$N_{\text{mbs}}^{>0}$	% zero
2	3	2	0	2	00.00
3	9	7	2	5	28.57
4	18	34	18	16	52.94
5	30	192	133	59	69.27
6	45	1206	959	247	79.52
7	63	8033	6922	1111	86.17
8	84	55974	50680	5294	90.54

The first nonzero-weight many-body configurations for  $N$  particles at  $\nu = 1/3$  have the form  $|0, 3, \dots, 3(N-1)\rangle$ , e.g.,  $|0, 3, 6, 9, 12, 15, 18\rangle$  for seven particles. The angular momenta of individual particles in these states are  $L_j = 3(j-1)$  for  $j = 1, \dots, N$ . The largest angular momentum of individual particles in all possible many-body configurations which contribute to the Laughlin function equals  $L_{\text{max}} = L_N = 3(N-1)$ . In general, if  $\nu = 1/m$  in Eq. (5),  $m = 3, 5, 7$ , then  $L_{\text{max}} = L_N = m(N-1)$ .

Having obtained the expansion coefficients  $C_s$ ,  $D_s$  and  $A_s^{\text{RL}}$  for different numbers of particles one can now calculate physical properties of the Laughlin state (79).

### C. Energy of the Laughlin state

The energy of the Laughlin state is determined by the formula (the constant kinetic energy contribution  $N\hbar\omega_c/2$  is omitted)

$$E_{\text{RL}}(N) = \langle \Psi_{\text{RL}} | \hat{\mathcal{H}} | \Psi_{\text{RL}} \rangle = \sum_{s=1}^{N_{\text{mbs}}} \sum_{s'=1}^{N_{\text{mbs}}} A_s^{\text{RL}} A_{s'}^{\text{RL}} \langle \Psi_s | \hat{V}_{bb} + \hat{V}_{eb} + \hat{V}_{ee} | \Psi_{s'} \rangle \quad (93)$$

in which all required matrix elements are calculated above. The calculated values of the energy (93), as well as the energy differences  $E_{\text{RL}} - E_{\text{GS}}$  between the Laughlin state and the true ground state are given in Table IV in the last two columns. The difference  $E_{\text{RL}} - E_{\text{GS}}$  increases significantly with the growth of  $N$  (by more than 90 times when  $N$  changes from  $N = 2$  to  $N = 7$ ), see Figure 10(a). In order to quantitatively estimate how big the deviation of the Laughlin energy from the true ground state energy is, I introduce a dimensionless quantity

$$\eta = \frac{E_{\text{RL}} - E_{\text{GS}}}{E_{\text{1st}} - E_{\text{GS}}} \quad (94)$$

which measures the difference  $E_{\text{RL}} - E_{\text{GS}}$  in units of the energy gap between the true first excited state and the true ground  $E_{\text{1st}} - E_{\text{GS}}$ . The value of  $\eta$  is plotted as a function of  $N$  in Figure 10(b). For  $N = 4, 5$  and  $7$  the value of  $\eta$  is greater than 1, i.e. the energy of the Laughlin state is not only greater than the energy of the ground state, which is understandable for the trial wave function, but also greater than the energy of the first excited state. For  $N = 7$ , the value of  $\eta$  equals 5.8825 at  $\nu = 1/3$ .

For  $N = 6$ , the wave functions of the Laughlin and the true ground states are accidentally close to each other; this can be seen from the comparison of the electron densities in both states in Section V E. This is the reason why both the absolute and relative energy differences between the Laughlin and the true ground states are smaller at  $N = 6$  compared to neighboring values of  $N$ .

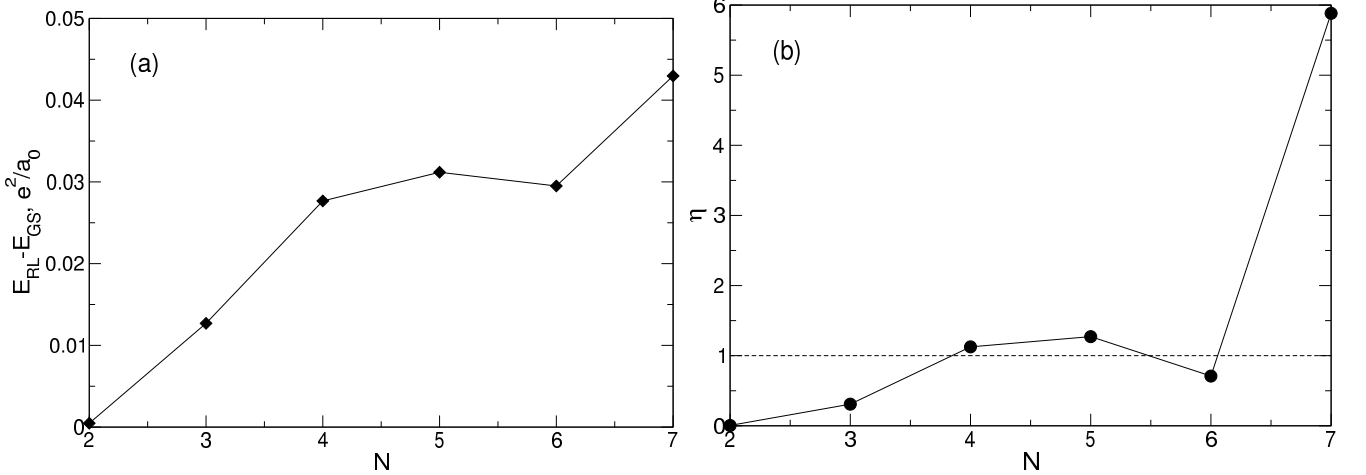


FIG. 10. (a) The energy difference between the Laughlin state and the true ground state of a system of  $N$  particles as a function of  $N$ ; the energy unit is  $e^2/a_0$ . (b) The value of  $\eta$  defined by Eq. (94), as a function of  $N$ .

#### D. Deviation of the Laughlin wave function from the true ground state wave function

The energy difference between the Laughlin state and the exact ground state is very large. How big is the discrepancy between the wave functions? Figure 11 shows the expansion coefficients of the true ground state wave function and the Laughlin wave function,  $A_s^{\text{GS}}$  and  $A_s^{\text{RL}}$ , for several many-body basis states, in the intervals  $4482 \leq s \leq 4496$  and  $3230 \leq s \leq 3290$  selected as examples. One sees a large difference between the vectors  $A_s^{\text{GS}}$  and  $A_s^{\text{RL}}$ . In the first example, Figure 11a, both coefficients are finite, and  $A_s^{\text{GS}}$  can be almost twice as big as  $A_s^{\text{RL}}$ . For example, for  $s = 4493$  and  $4494$  (the states  $|0, 7, 9, 10, 11, 12, 14\rangle$  and  $|0, 8, 9, 10, 11, 12, 13\rangle$ ) the ratio  $A_s^{\text{GS}}/A_s^{\text{RL}}$  equals 1.819 and 1.858, respectively. In the second example, Figure 11b, the coefficients  $A_s^{\text{GS}}$  of all  $\sim 60$   $s$ -states are on the order of 0.005 – 0.01, while the Laughlin coefficients  $A_s^{\text{RL}}$  for these states are identically zero.

In order to quantitatively characterize the overall discrepancy between the states  $\Psi_{\text{GS}}$  and  $\Psi_{\text{RL}}$ , I calculate the standard deviation

$$D = \sqrt{\sum_{s=1}^{N_{\text{mbs}}} (A_s^{\text{GS}} - A_s^{\text{RL}})^2} \quad (95)$$

Table XI shows the quantity  $D$  for  $N$  varying from  $N = 2$  up to  $N = 7$ . The second column of Table XI shows the

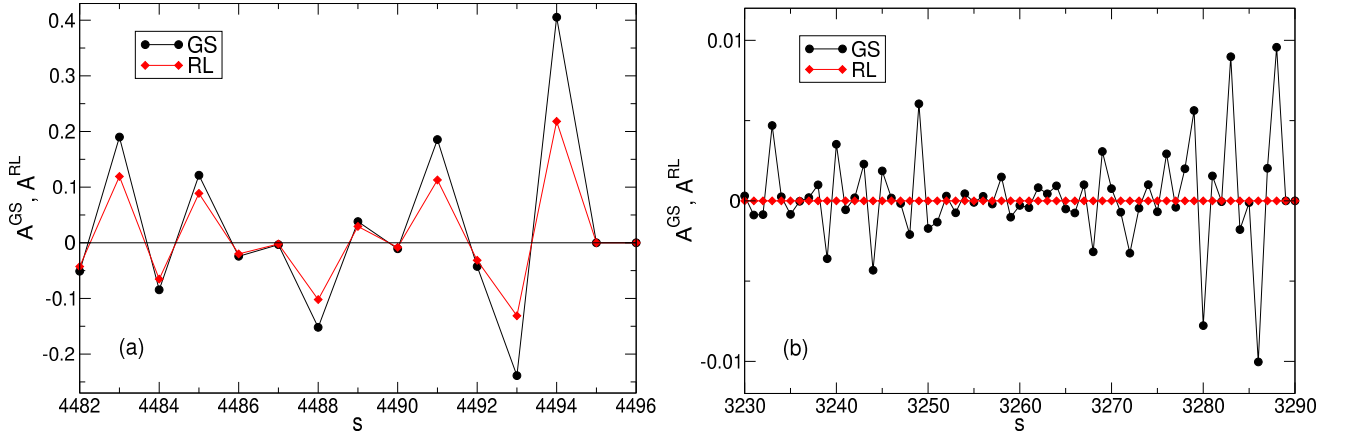


FIG. 11. The expansion coefficients  $A_s^{\text{GS}}$  and  $A_s^{\text{RL}}$  of the true ground state wave function (55) and of the Laughlin wave function (81) for a few selected many-body basis states: (a)  $4482 \leq s \leq 4496$  and (b)  $3230 \leq s \leq 3280$ . The Landau level filling factor is  $\nu = 1/3$ , the number of particles is  $N = 7$ , the total angular momentum is  $\mathcal{L} = 63$ , and the total number of many-body basis states is  $N_{\text{mbs}} = 8033$ .

projection of the Laughlin wave function onto the true ground state

$$P = \langle \Psi^{\text{RL}} | \Psi^{\text{GS}} \rangle = \sum_{s=1}^{N_{\text{mbs}}} A_s^{\text{RL}} A_s^{\text{GS}} = 1 - D^2/2. \quad (96)$$

For  $N = 2$  the deviation (95) is quite small, about 3.3%, but as  $N$  increases, it substantially grows and exceeds  $\sim 40\%$  for  $N = 7$ . It is highly unlikely that this trend will be reversed with a further increase in the number of particles.

TABLE XI. The standard deviation (95) and the projection (96) of the Laughlin wave function (79) from/onto the ground state wave function (55) at  $\nu = 1/3$ .

$N$	$D$	$P$
2	0.0334	0.9994
3	0.1755	0.9846
4	0.2978	0.9557
5	0.3500	0.9387
6	0.2960	0.9562
7	0.4021	0.9191

### E. Electron density in the Laughlin state

The density of electrons in the Laughlin state (79) at  $\nu = 1/3$  is determined by the formula similar to (65),

$$n_e^{\text{RL}}(r) = \sum_{s=1}^{N_{\text{mbs}}} (A_s^{\text{RL}})^2 \sum_{j=1}^N |\psi_{L_j^{(s)}}(\mathbf{r})|^2. \quad (97)$$

The normalized density (97) is shown in Figure 12(a) for  $2 \leq N \leq 8$ . At  $N \leq 4$  my results coincide with those obtained by Ciftja et al. in Ref. [22] by a different method. At larger  $N$ , the Laughlin density behaves qualitatively similarly to the exact electron density if  $N \lesssim 5$ : both have a maximum at a finite  $r$ , and this maximum shifts to a larger  $r$  as  $N$  increases. However, quantitatively, the density difference at  $r/a_0 \ll 1$  becomes very large already at  $N \geq 3$ , see Figure 12(b): while at  $N = 2$  the Laughlin density differs from the exact one “only” by  $\sim 8.5\%$ , at  $N = 3$  the difference is already about 34%, and at  $N = 4$  and 5 it approaches 50%. At  $N = 6$  the densities of electrons in the both states become close to each other, but this is a coincidental result of two different trends. While for Laughlin electrons  $n_{\text{RL}}(r \ll a_0)/n_s$  tends to unity at  $N \rightarrow \infty$ , Ref. [20, 21], the ratio  $n_{\text{GS}}(r \ll a_0)/n_s$  is close to 1 only because

the maximum in the disk center is not yet sufficiently developed. When  $N$  grows further, the local density difference becomes huge approaching  $\sim 70\%$  for  $N = 7$  at  $r \ll a_0$ , and the coordinate dependencies of the exact and Laughlin densities becomes *qualitatively* different, see Figure 12(c). While the exact density shows the formation of a structure resembling a sliding Wigner crystal, with a large density maximum arising in the disk center, the Laughlin density flattens out in the inner part of the disk.

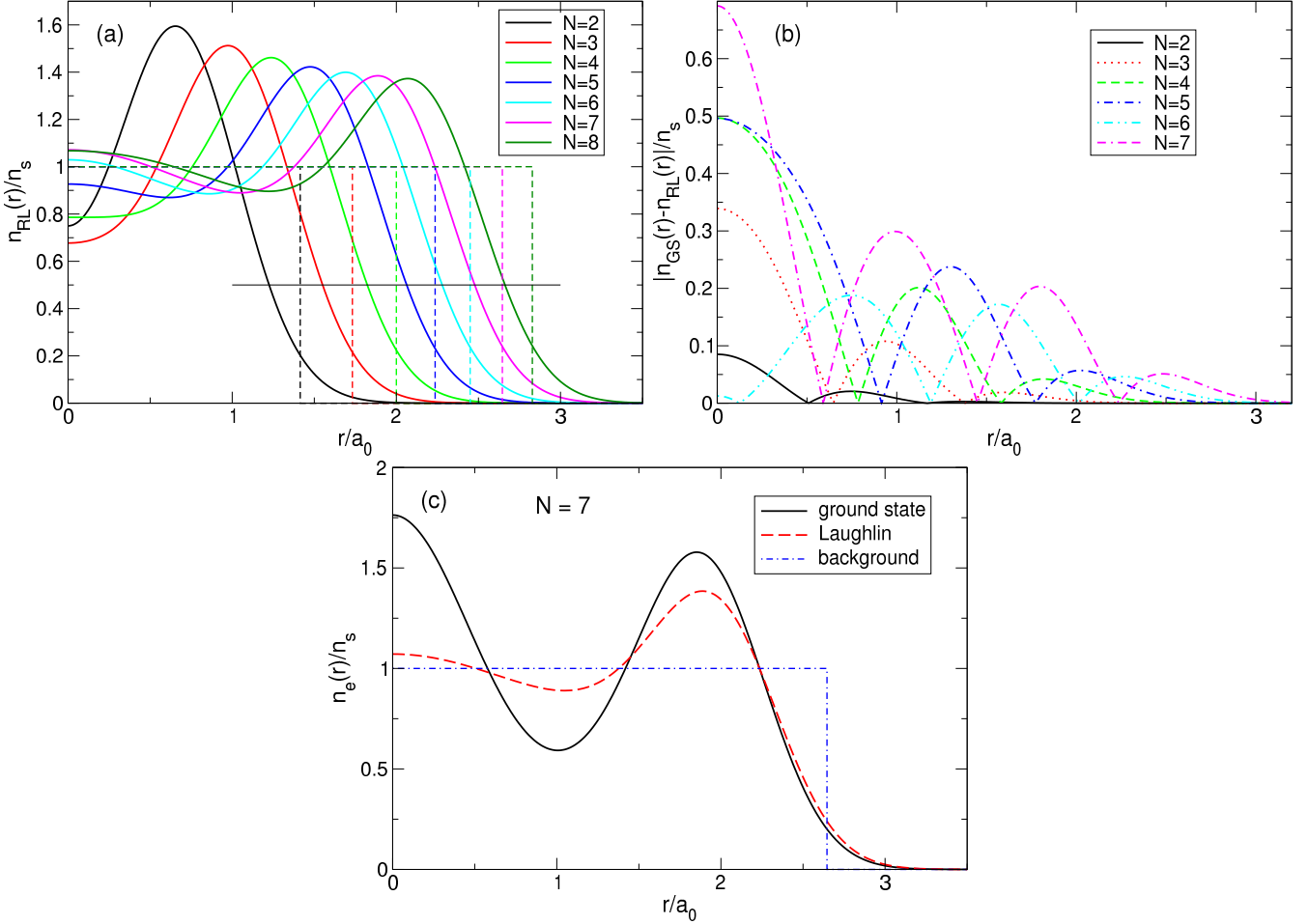


FIG. 12. (a) The density of electrons (solid curves) in the Laughlin state (79) at  $\nu = 1/3$ , as a function of the radial coordinate for  $N = 2$  to 8. The dashed lines show the corresponding positive background densities; the thin horizontal black line indicates the level 0.5, which determines the radii of the electron disks. (b) The absolute value of the density difference between the true ground state and the Laughlin state for different  $N$ . (c) The density of electrons in the true ground and Laughlin states at  $N = 7$ .

#### F. Pair correlation function in the Laughlin state

The pair correlation function  $P_{RL}(\mathbf{r}, \mathbf{r}')$  in the Laughlin state  $\nu = 1/3$  can be calculated using a formula similar to (66); only the coefficients  $A_s^{GS}$  should be replaced by  $A_s^{RL}$ . In general, the function  $P_{RL}(\mathbf{r}, \mathbf{r}')$  looks similarly to the plots of Figure 6. But there exists a very large quantitative difference at small  $|\mathbf{r} - \mathbf{r}'|$ , when  $|\mathbf{r} - \mathbf{r}'|/a_0 \lesssim 0.6$ , see Figure 13. While the exact pair correlation function tends to zero at  $|\mathbf{r} - \mathbf{r}'| \rightarrow 0$  as  $P_{GS}(\mathbf{r}, \mathbf{r}') \propto |\mathbf{r} - \mathbf{r}'|^2$ , the Laughlin pair correlation function vanishes as  $P_{RL}(\mathbf{r}, \mathbf{r}') \propto |\mathbf{r} - \mathbf{r}'|^6$  at  $|\mathbf{r} - \mathbf{r}'| \rightarrow 0$ . This is a direct consequence of the unphysical assumption in (79), that the wave function contains only the polynomials  $(z_j - z_k)^3$ . In the real world this is not the case, see the additional discussion of this point in Section V J.

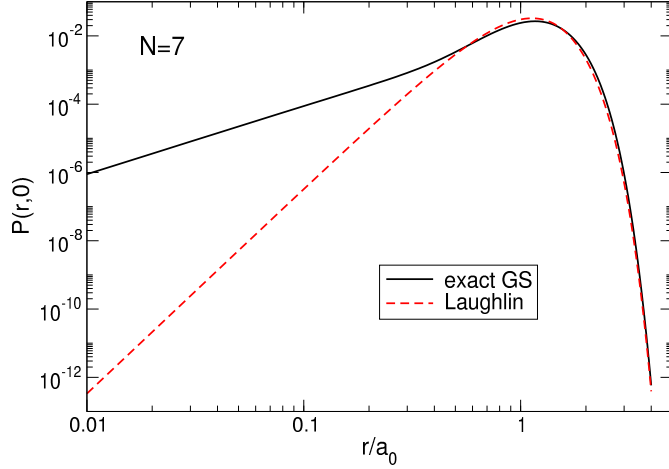


FIG. 13. The pair correlation functions  $P(\mathbf{r}, \mathbf{0})$  for the exact ground state and the Laughlin state, for a system of  $N = 7$  particles.

#### G. Additional remark to the case of $N = 7$ particles

Results obtained for the energy of the ground and the first excited states of a seven-electron system need a little more discussion. Laughlin suggested [6] that the ground state of an  $N$ -particle system at  $\nu = 1/3$  should have the total angular momentum  $\mathcal{L} = 3N(N - 1)/2$ . For  $N = 7$  this is  $\mathcal{L} = 63$ . My exact results show that the ground state of the seven-particle system has the angular momentum  $\mathcal{L} = 63$  indeed, while the first excited states has the angular momentum  $\mathcal{L} = 57$ , Table IV. The difference between the energies of the first excited and the ground state equals  $E_{1st} - E_{GS} = 0.0073e^2/a_0$ .

However, Kasner et al. [18] also performed exact diagonalization calculations for  $N$  electrons in the disk geometry. Their calculations showed that the ground state of the seven-particle system at  $\nu = 1/3$  has the angular momentum  $\mathcal{L} = 57$ . This *exact* result contradicted the variational theory of Laughlin, but the authors of [18] could not resolve this “dilemma” and decided just to “disregard this difficulty”.

Questions arise: Why the exact results of Ref. [18] contradict my exact results and the assumption of Laughlin? Were the results of Ref. [18] correct?

This “dilemma” has a simple explanation. In the present paper I solve the problem for the positive background density having the step-like form (15). The step-like profile model was chosen in order to be able to quantitatively compare results of my work with those of Laughlin [6] and some other authors [20, 21] who also used this model for the background charge density. But this choice of the density profile model is not unique. Kasner et al. [18] assumed that the positive charge density profile has a *smooth* edge and is described by the formula coinciding with the density of electrons in the MDD state, see Eqs. (71)–(72) and the black curve in Figure 8. I have also done calculations for this density profile and confirm the results of Ref. [18]. For the smooth density profile (71)–(72) and  $N = 7$  I have found at  $\nu = 1/3$  that

$$\left\{ \begin{array}{l} E_{GS} = E_0^{3\mathcal{L}_{\min} - \delta\mathcal{L}} = E_0^{\mathcal{L}=57} = -6.679511889, \\ E_{1st} = E_0^{3\mathcal{L}_{\min}} = E_0^{\mathcal{L}=63} = -6.661383414, \\ E_{RL} = -6.636383519, \end{array} \right. \quad (98)$$

in units  $e^2/a_0$ . The energy difference between the true first excited state (now  $\mathcal{L} = 63$ ) and the true ground state (now  $\mathcal{L} = 57$ ) is  $E_{1st} - E_{GS} = 0.018128475e^2/a_0$ , while the energy difference between the Laughlin state and the true ground state is  $E_{RL} - E_{GS} = 0.04312837e^2/a_0$ . The factor  $\eta$ , defined by Eq. (94), for the smooth profile is  $\eta = 2.379$ . Notice that for the smooth profile the projection of the Laughlin wave function onto the true ground state wave function is zero, since these functions have different angular momenta  $\mathcal{L}$  and are therefore orthogonal.

#### H. About the variational principle in the thermodynamic limit

In Section IB, I have proved that the variational principle is useless in the thermodynamic limit. While it may give a correct estimate for the ground state energy per particle, it does not help to determine the correct ground state

wave function. Let me illustrate this with a simple quantitative example.

In Section IV I have analyzed the properties of the MDD configuration  $|\Psi_{\text{mdd}}\rangle = |0, 1, \dots, N-1\rangle$ , Eq. (67), in particular the energy, Figure 7, and the density, Figure 8, of this state. If only the lowest Landau level single-particle states are considered, the MDD configuration is the ground state of the system at  $\nu = 1$ .

Now I take two other quantum states, which I will call “MDD-plus” and “MDD-shift”. The MDD-plus state  $|\Psi_{\text{mdd}}^+\rangle = |0, 1, \dots, N-2, N\rangle$  differs from  $|\Psi_{\text{mdd}}\rangle$  by the angular momentum of only one,  $N$ -th electron:  $L_N = N-1 \rightarrow L_N = N$ . In the MDD-shift state,  $|\Psi_{\text{mdd}}^{\Rightarrow}\rangle = |1, 2, \dots, N-1, N\rangle$ , individual angular momenta of all particles are increased by one as compared to their MDD  $L$ 's:  $L_j = j-1 \rightarrow L_j = j$ ,  $j = 1, \dots, N$ . The total angular momenta of the plus- and shift-states are  $\mathcal{L} = N(N-1)/2 + 1$  and  $\mathcal{L} = N(N+1)/2$  respectively, and hence, these two states are orthogonal to the ground MDD state: their projections onto the ground state are zero. What are the energy and the density of these two configurations? This question can be easily answered for any  $N$  with the help of the formulas obtained above.

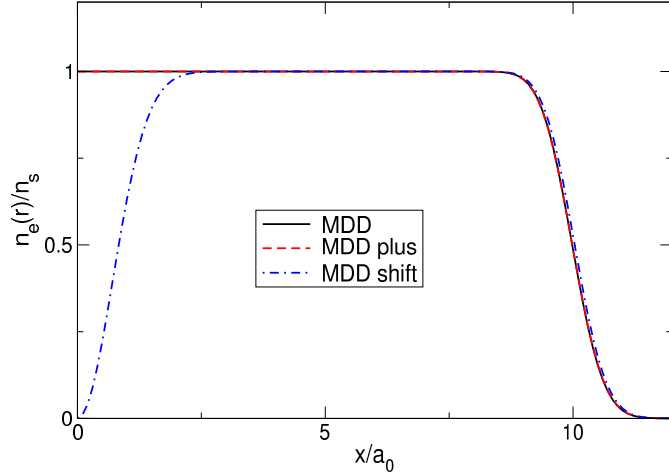


FIG. 14. The density of electrons in the MDD, MDD-plus, and MDD-shift states as a function of  $r/a_0$  for  $N = 100$ .

Figure 14 shows the electron density in the MDD, MDD-plus, and MDD-shift states. The densities of the first two states are very close to each other. But the density of the MDD-shift state has a deep hole in the disk center and differs significantly from both the MDD and MDD-plus states. If we knew nothing about the ground state of the system, we would definitely exclude the MDD-shift state from the list of potential candidates for the ground state wave function, because it does not give a physically reasonable coordinate dependence of the electron density.

What about the energy of these three states? Figure 15(a) shows the energy per particle of the MDD, MDD-plus, and MDD-shift configurations, as a function of  $1/\sqrt{N}$ , for  $N$  varying from 1 to 100. One sees that at small  $N$  the energy difference between the both excited and the ground (MDD) states is very large, but when  $N$  grows, this difference quickly tends to zero. Figure 15(b) shows the energy differences  $\delta E_{\text{mdd}}^+/N$  and  $\delta E_{\text{mdd}}^{\Rightarrow}/N$  in dependence of  $1/N$ . In spite of the MDD-shift state has an evidently incorrect coordinate dependence of the electron density, both differences tend to zero linearly with  $1/N$ , which implies that  $\delta E_{\text{mdd}}^+$  and  $\delta E_{\text{mdd}}^{\Rightarrow}$  are constants at  $N \rightarrow \infty$ :  $\delta E_{\text{mdd}}^+ \approx 0.118050e^2/a_0$  and  $\delta E_{\text{mdd}}^{\Rightarrow} \approx 0.8973e^2/a_0$ . Obviously, there exist an infinite number of different wave functions whose energy per particle will tend to the same limit at  $N \rightarrow \infty$ . For example, the state  $|0, 1, 2, \dots, N-2, 5N\rangle$ , in which one electron is located far beyond the disk boundary, would also have the same energy per particle in the thermodynamic limit.

### I. Electron density in the Laughlin state at large $N$

The density of electrons in the MDD-shift state, Figure 14, is “physically unreasonable”, therefore, if the ground state of the system at  $\nu = 1$  was unknown, one could definitely exclude the state  $|\Psi_{\text{MDD}}^{\Rightarrow}\rangle$  from the list of potential candidates for the ground state wave function. Could one, for similar reasons, exclude the Laughlin wave function (5) from the list of potential candidates for the role of the ground state wave function at  $\nu = 1/m$ ? This question can be answered due to the studies of Ciftja and coauthors [20, 21], who calculated, using Monte Carlo simulations, the density of electrons  $n_e^{\text{RL}}(r)$  in the  $\nu = 1/3$  Laughlin states for  $N = 64, 100, 144$ , and  $196$  [20], and in the  $1/5$  and  $1/7$  states for  $N = 196$  [21].

As seen in Figure 12(a), the normalized Laughlin density at small  $r$  tends to unity as  $N$  increases, and has a rather large peak near the edge of the disk at  $r \approx R - a_0$ . The value of the normalized density  $n_e^{\text{RL}}/n_s$  in this peak varies

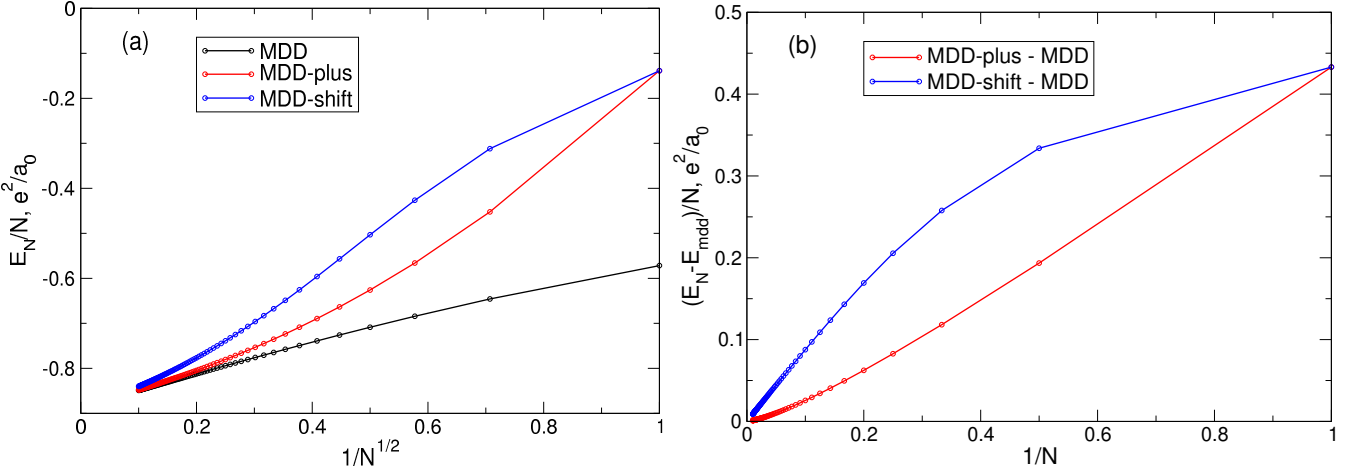


FIG. 15. (a) The energy of the MDD, MDD-plus, and MDD-shift states, as a function of  $1/\sqrt{N}$ . (b) The energy differences as a function of  $1/N$ .

from  $\sim 1.6$  for  $N = 2$  to  $\sim 1.37$  for  $N = 8$ . Do these peculiarities remain when  $N$  grows further? Figure 16 shows results of Refs. [20, 21] (curves with symbols) replotted as a function of  $r/a_0$  (in contrast to Refs. [20, 21], where these data are plotted in dependence of  $r/l_B$ , I use more convenient  $B$ -independent length and energy units). At  $r/a_0 \lesssim 11$  (not shown in Figure 16) the normalized density  $n_e^{\text{RL}}/n_s$  calculated in Refs. [20, 21] is very close to 1, which agrees with the Laughlin statement that his function describes a uniform liquid. However, near the disk edge this “liquid” becomes strongly inhomogeneous. The ring of the high electron density, which has been seen at  $N \leq 8$  in Figure 12, is also preserved at  $N$  up to  $N = 196$ , see Fig. 3 in Ref. [20] and Fig. 1 in Ref. [21]. Consider this Laughlin state feature in more detail.

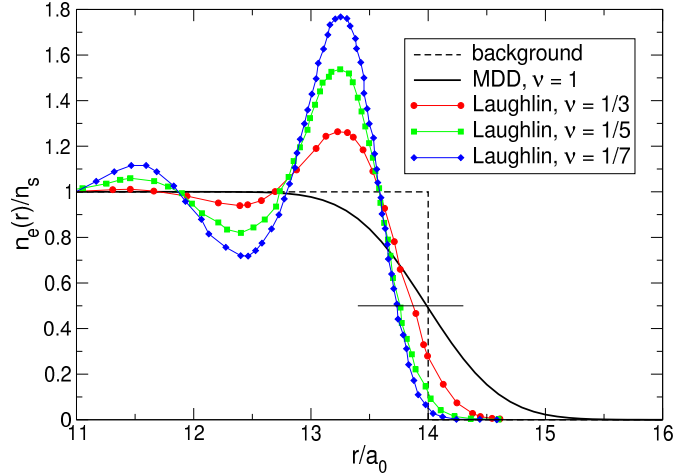


FIG. 16. The coordinate dependencies of the density of electrons in the Laughlin states (5) at  $\nu = 1/3, 1/5$ , and  $1/7$ , calculated for  $N = 196$  by Ciftja et al. in Refs. [20, 21]; the discrete numerical data points are connected by lines to guide the eye. The thick black solid curve shows the MDD density at  $\nu = 1$ . At  $r/a_0 \lesssim 11$  (not shown in the Figure) the normalized electron density equals 1 according to Refs. [20, 21]. Thin horizontal line at the level 0.5 visualizes the change of the electron disk radius when  $\nu$  decreases from  $\nu = 1$  to  $\nu = 1/7$ .

It is possible to fit the numerical data of Ciftja et al. [20] for  $\nu = 1/\beta = 1/3$  by a linear combination

$$\frac{n_e^{\text{fit}}(r)}{n_s} = \sum_{L=0}^{L_{\text{max}}(N)} \Phi_L \left( \sqrt{\beta} \frac{r}{a_0} \right) + \sum_{k=1}^3 (-1)^{k-1} A_k(N) \Phi_{L_k(N)} \left( \sqrt{\beta} \frac{r}{a_0} \right) \quad (99)$$

of functions

$$\Phi_L(x) = \frac{x^{2L}}{L!} e^{-x^2}, \quad (100)$$

which are related to the single-particle states (13),

$$|\psi_L(\mathbf{r})|^2 = \frac{1}{\pi\lambda^2} \Phi_L\left(\frac{r}{\lambda}\right). \quad (101)$$

The angular momenta  $L_{\max}(N)$  and  $L_k(N)$ , as well as the coefficients  $A_k(N)$  in Eq. (99) are

$$L_{\max}(N) = 3N - 1 - \sqrt{N}, \quad L_k(N) = 3N - 2(3k - 1)\sqrt{N} - 13 + 12k, \quad (102)$$

$$A_1(N) = 1.205\sqrt{N} + 0.07, \quad A_2(N) = 0.2525\sqrt{N} - 0.115, \quad A_3(N) = \sqrt{N} - A_1(N) + A_2(N). \quad (103)$$

The fitting function (99) is not unique and not exact, but it very well fits the numerical data [20], see Figure 17. Remarkably, the data for different  $N$  can be equally well fitted by a single formula (99), which implies that Eq. (99) should also successfully work at even larger  $N$ , in the thermodynamic limit.

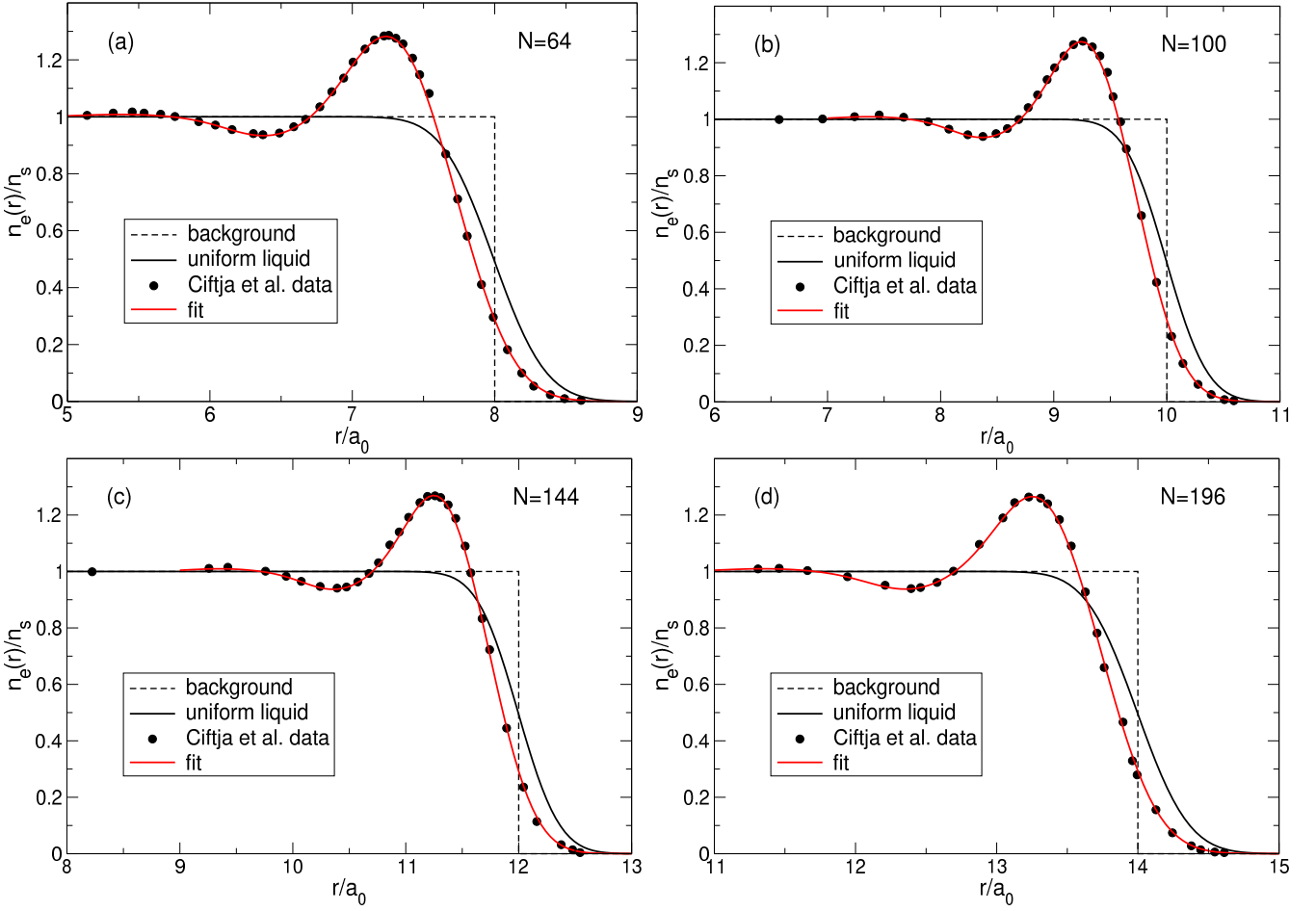


FIG. 17. Fitting of the numerical data [20] for the density of electrons in the  $\nu = 1/3$  Laughlin state by the analytical function (99) for (a)  $N = 64$ , (b)  $N = 100$ , (c)  $N = 144$ , and (d)  $N = 196$ .

Apart from the data of Ref. [20] and the fitting function (99), I also show in Figures 17(a)-(d), by black solid lines, the density of a “uniform liquid”

$$\frac{n_e^{\text{UL}}(r)}{n_s} = \sum_{L=0}^{\beta N-1} \Phi_L\left(\sqrt{\beta} \frac{r}{a_0}\right) = Q(\beta N, \beta r^2/a_0^2), \quad (104)$$

which is similar to the density of the MDD state (71) but is defined for  $\beta = 1/\nu = 3$ . The function (104) satisfies the condition

$$\int_0^{2\pi} d\phi \int_0^\infty r dr n_e^{\text{UL}}(\mathbf{r}) = N \quad (105)$$

and is ideally flat at  $r \lesssim R - a_0$ . As seen from Figures 17(a)-(d), the radius of the electron disk in the “uniform liquid” state (104), defined as the point where  $n_e^{\text{UL}}(r)/n_s = 1/2$ , is very close to the radius  $R = a_0\sqrt{N}$  of the positively charged background disk.

If the Laughlin wave function (79) really described a homogeneous liquid state, it would have to have a density close to (104). But, as seen from Figures 17(a)-(d), the radii of the electron disks in the Laughlin state (79) is always noticeably smaller than the radii of the “uniform liquid” and of the positive background. Since all densities should satisfy the electroneutrality condition (105), the decrease in diameter of the “Laughlin liquid” disk should be compensated by a strong increase in the “Laughlin liquid” density in the interior of the system. This is indeed the case, that is the Laughlin state (79) describes a strongly inhomogeneous state of the system.

Mathematically, one can evaluate this redistribution of the electron density by comparing the “uniform liquid” density (104) with the “Laughlin liquid” density, calculated for large  $N$  in Ref. [20] and fitted by the formula (99). The “uniform liquid” density consists of a sum of the functions  $\Phi_L$  with  $L$  running from  $L = 0$  up to  $L = 3N - 1$ . The “Laughlin liquid” density also contains a similar sum, but  $L$  in the first term of Eq. (99) runs from  $L = 0$  up to  $L = L_{\text{max}} = 3N - 1 - \sqrt{N}$ , Eq. (102). A *macroscopically* large number ( $\propto \sqrt{N}$ ) of the  $L$ -states are lost from the Laughlin function. To compensate this loss and to describe the oscillating behavior of the Laughlin density near the edge of the disk, three additional terms with large amplitudes  $A_k(N) \propto \sqrt{N}$ , Eq. (103), have to be added to the fitting function (99). Notice that the high density ring lies approximately at  $R - 1.2a_0 \lesssim r \lesssim R - 0.4a_0$ , with the density maximum at  $r \approx R - 0.8a_0$ , that is all changes in the local electron density occur inside the sample, at  $r \lesssim R - a_0$ , which means that they also take place in the thermodynamic limit  $N \rightarrow \infty$ .

The above discussion refers to the case  $\nu = 1/3$ . At  $\nu = 1/5$  and  $1/7$  the Laughlin function (5) demonstrates even stronger inhomogeneity of the local electron density near the edge of the system, see Figure 16. The electron disk radius becomes smaller, and the maximum of the electron density near  $r \approx R - 0.8a_0$  gets higher. Thus, not only is the Laughlin state characterized by a non-physical feature of a strongly inhomogeneous density, but, in addition, this inhomogeneity depends significantly on the magnetic field.

Imagine that one has a macroscopic 2DEG sample with an electron density on the order of  $10^{11} \text{ cm}^{-2}$  [3]. In equilibrium at  $B = 0$  the sample is locally electroneutral, i.e. the density of electrons equals the density of the positive background at any point. Now one switches the magnetic field on and increases it up to the value  $\sim 50 \text{ kG}$  [3] corresponding to the Landau level filling factor  $\nu = 1$ . One gets the MDD ground state with a perfectly uniform density of electrons (71) at all  $r \lesssim R - a_0$ , Figure 18(a). Then one increases the magnetic field further, up to  $\sim 150 \text{ kG}$  [3] which corresponds to the filling factor  $\nu = 1/3$ . If the Laughlin wave function (5) corresponded to reality, a ring with a strongly enhanced electron density ( $\sim 1.27 \times 10^{11} \text{ cm}^{-2}$ ) would have to grow near the edge of the sample, Figure 18(b). If after that the  $B$ -field is increased further, up to  $\nu = 1/5$  and  $\nu = 1/7$ , then the local electron density in the edge ring should increase to  $\sim 1.55 \times 10^{11} \text{ cm}^{-2}$  and  $\sim 1.77 \times 10^{11} \text{ cm}^{-2}$  respectively, see Figures 18(c) and (d).

Such a strong redistribution of the electron density would require enormous energy costs, which can be estimated as follows. The density of the uncompensated charge can be modeled as

$$\delta\rho(\mathbf{r}) = \gamma e n_s \Theta(R - r) \Theta(r - R + a_0) \quad (106)$$

where  $\gamma$  is a number on the order of unity:  $\gamma \approx 0.27$ ,  $0.55$ , and  $0.78$  at  $\nu = 1/3$ ,  $1/5$ , and  $1/7$ , respectively. The electrostatic energy of this uncompensated charge is

$$\delta E = \int \frac{\delta\rho(\mathbf{r})\delta\rho(\mathbf{r}')}{|\mathbf{r} - \mathbf{r}'|} d\mathbf{r} d\mathbf{r}' = \int \frac{d\mathbf{q}}{2\pi q} |\delta\rho_{\mathbf{q}}|^2, \quad (107)$$

where the Fourier transform of  $\delta\rho(\mathbf{r})$  equals

$$\delta\rho_{\mathbf{q}} = \frac{2\pi\gamma e n_s}{q^2} q R \left( (1 - \xi) J_1(qR(1 - \xi)) - J_1(qR) \right), \quad (108)$$

and

$$\xi = \frac{a_0}{R} = \frac{1}{\sqrt{N}} \quad (109)$$

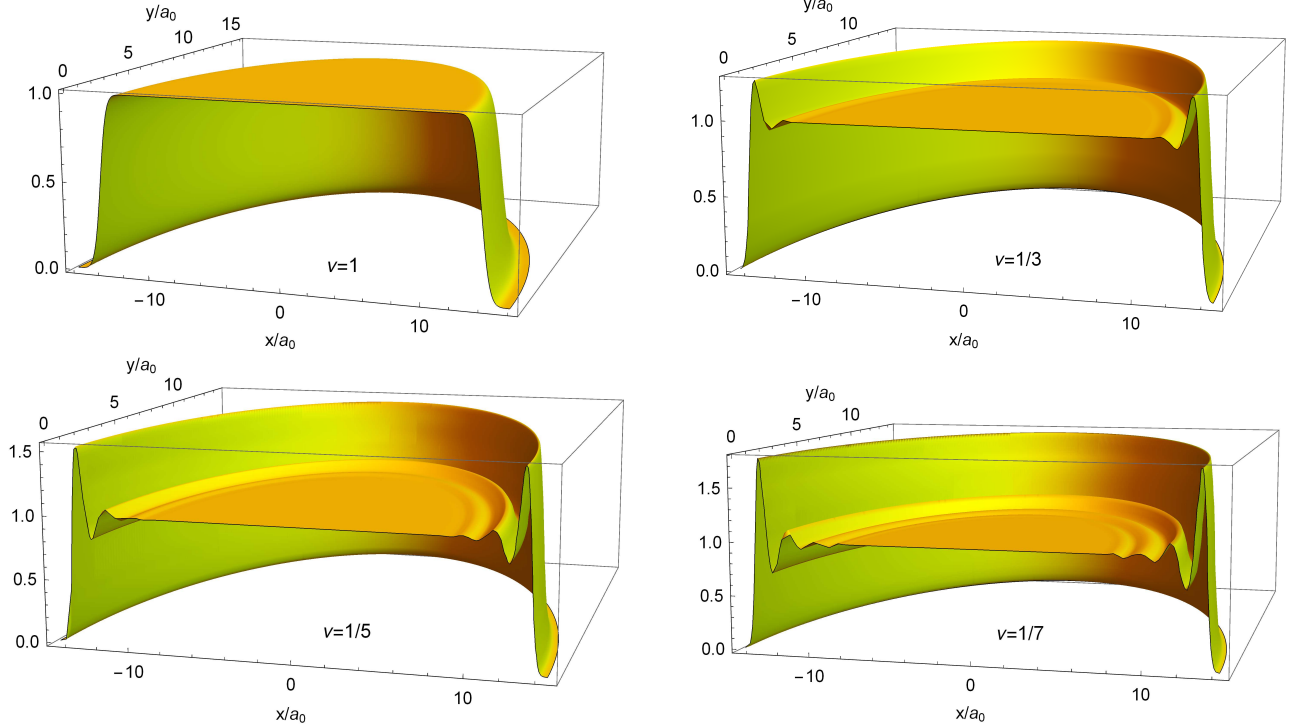


FIG. 18. The density of electrons in the MDD ( $\nu = 1$ ) and in the Laughlin states (5) with  $\nu = 1/3$ ,  $1/5$  and  $1/7$ . The number of particles is  $N = 196$ . The data for the Laughlin electron densities are taken from Refs. [20, 21].

is a small parameter. Substituting (108) into (107) gives in the limit  $\xi \ll 1$  ( $N \gg 1$ )

$$\delta E \approx \frac{e^2}{R} (2\gamma N)^2 \frac{\xi^2}{2\pi} \left( 3 + 2 \ln \frac{8}{\xi} \right) = \left( \frac{e^2}{a_0} \frac{6\gamma^2}{\pi} \right) \sqrt{N} \left[ 1 + \frac{1}{3} \ln (64N) \right]. \quad (110)$$

The electrostatic energy (110) grows as  $\sqrt{N} \ln(N)$  in the thermodynamic limit. If the density of electrons assumes a typical value  $n_s = 3 \times 10^{11} \text{ cm}^{-2}$  and the dielectric permittivity, which should be taken into account here, is  $\epsilon = 12.8$ , the energy  $(e^2/a_0\epsilon)(6\gamma^2/\pi)$  equals 1.52 meV for  $\nu = 1/3$  ( $\gamma = 0.27$ ). Then for the macroscopic number of particles  $N \simeq 10^{11}$  the electrostatic energy (110) exceeds 2.5 keV at  $\nu = 1/3$ ,  $\sim 10$  keV at  $\nu = 1/5$ , and about 20 keV at  $\nu = 1/7$ . The “Laughlin liquid” requires too much energy for its existence.

### J. Final remarks

Another reason why the Laughlin wave function is inappropriate for the description of the ground state of the FQHE system is as follows. The behavior of the many-body wave function at  $|\mathbf{r}_j - \mathbf{r}_k| \rightarrow 0$  is governed by the Coulomb interaction terms  $\sum_{jk} \Psi / |\mathbf{r}_j - \mathbf{r}_k|$  in the many-body Schrödinger equation. To compensate the  $1/r$ -singularity in this equation, the wave function should be proportional to  $|\mathbf{r}_j - \mathbf{r}_k|$  at  $|\mathbf{r}_j - \mathbf{r}_k| \rightarrow 0$ . This is indeed the case for the MDD solution at  $\nu = 1$  and the true ground state solution at  $\nu = 1/3$ . The Laughlin assumption  $\Psi_{\text{RL}} \propto |\mathbf{r}_j - \mathbf{r}_k|^m$  with  $m = 3, 5, 7$  actually suggests that Laughlin electrons repel each other substantially stronger than needed in the world of Coulomb forces, as if the electron-electron interaction potential were proportional to  $1/|\mathbf{r}_j - \mathbf{r}_k|^{m+1}$ . As a result, electrons are pushed out of the disk center, with forces proportional to  $1/|\mathbf{r}_j - \mathbf{r}_k|^{m+1}$ , and have to accumulate near the disk edge with a local electron density growing with  $m$ , see Figures 16 and 18.

Finally, a few words should be said about the excited states of the system. Laughlin asserted [6], without any rigorous proof, that the excitations of the system, quasi-electrons and quasi-holes, are described by wave functions that differ from (5) by additional polynomial factors of the type  $\prod_i (z_i - z_0)$ . According to [6], these excitations are particles of charge  $1/m$ ,  $m = 3, 5, 7$ . Exact calculations show that there are no grounds for such statements. As can be seen from Figure 3, the excited states of the system are also similar to a floating Wigner crystal, the parameters of which, however, are slightly different from those of the ground state. There are no hints of the existence of any fractionally charged quasi-particles in the exact solution of the problem.

## VI. SUMMARY AND CONCLUSIONS

This paper consists of two large parts. In the first part I have developed an exact diagonalization theory for solving the many-body Schrödinger equation for  $N$  Coulomb-interacting 2D electrons at the lowest Landau level, in the presence of the neutralizing positive background in the shape of a disk. This theory is valid, in principle, for any number of particles and all Landau level filling factors  $\nu \leq 1$ , under the assumption that the contribution of states from the higher Landau levels can be neglected. I have presented complete analytical results for the ground and excited states energies and other physical properties of the FQHE systems of up to  $N = 7$  electrons at the Landau level filling factor  $\nu = 1/3$ . These results show that the ground states of the  $N$ -electron systems with  $N \leq 7$  at  $\nu = 1/3$  have the form resembling sliding Wigner molecules, which fully agrees with the classical solution of the problem [5].

Since for the last 40 years it was believed that the ground state of the FQHE system at  $\nu = 1/3$  is an incompressible homogeneous Laughlin fluid (5), I devoted the second part of this paper to a detailed analysis of the Laughlin state. I have calculated the energy and other physical properties of the Laughlin state (5) for  $N \leq 8$  and have shown that there exists a very large discrepancy between the physical properties of the Laughlin state and those of the true ground state. I have also shown that the creation of a Laughlin liquid would require enormous energy (on the keV scale in a typical macroscopic sample) due to violation of local electroneutrality, and that the main Laughlin's argument, that the energy per particle of the state (5) is the lowest in the thermodynamic limit, does not prove that the Laughlin function describes the ground state of the system, because one can indicate an infinite number of different trial wave functions which give the same variational energy at  $N \rightarrow \infty$ .

On the basis of these and other results obtained in this work I conclude that the Laughlin wave function (5) describes a fictitious state that cannot exist in nature. The “new state of matter” [6] – a homogeneous incompressible liquid, together with its fractionally charged excitations – does not correspond to physical reality. The interpretation of experimental results [23–25] on the observation of fractionally charged quasi-particles in the FQHE regime raise serious doubts, since there are no theoretical prerequisites for their existence.

## ACKNOWLEDGMENTS

The author thanks Elliott Lieb for useful discussions, Orion Ciftja for providing details and additional information about his works published in Refs. [20–22], Blagoje Oblak for a useful remark, and Nadya Savostyanova for reading the manuscript and useful comments on it.

## Appendix A: Matrix elements of the background-electron interaction energy

The formulas derived here are obtained for the step-like density profile (15).

### 1. General formulas

The matrix elements of the background-electron interaction energy are determined by Eq. (37). Substituting in that formula the Fourier transforms of the background and electron densities from Eqs. (17) and (35) and replacing the variable  $q\lambda/2 = x$  I obtain

$$\langle \Psi_s | \hat{V}_{be} | \Psi_{s'} \rangle = -\delta_{ss'} \frac{e^2}{R} 2N \sum_{j=1}^N \int_0^\infty \frac{dx}{x} J_1(x2R/\lambda) e^{-x^2} L_{L_j^{(s)}}^0(x^2). \quad (\text{A1})$$

Using the definition of the Laguerre polynomials,

$$L_n^l(x) = \sum_{m=0}^n (-1)^m \binom{n+l}{m+l} \frac{x^m}{m!}, \quad (\text{A2})$$

I get

$$\langle \Psi_s | \hat{V}_{be} | \Psi_{s'} \rangle = -\delta_{ss'} \frac{e^2}{R} 2N \sum_{j=1}^N \sum_{m=0}^{L_j^{(s)}} \binom{L_j^{(s)}}{m} \frac{(-1)^m}{m!} \int_0^\infty dx J_1(x2R/\lambda) e^{-x^2} x^{2m-1}. \quad (\text{A3})$$

The integral in this formula is known (Ref. [35], integral 2.12.9.3),

$$\int_0^\infty dx J_1(cx) e^{-x^2} x^{2m-1} = \frac{c}{4} \frac{\Gamma(m + \frac{1}{2})}{\Gamma(2)} {}_1F_1 \left( m + \frac{1}{2}, 2; -\frac{c^2}{4} \right), \quad (\text{A4})$$

so that I obtain

$$\langle \Psi_s | \hat{V}_{be} | \Psi_{s'} \rangle = -\delta_{ss'} \frac{e^2}{\lambda} N \sum_{j=1}^N \sum_{m=0}^{L_j^{(s)}} \binom{L_j^{(s)}}{m} \frac{(-1)^m}{m!} \Gamma \left( m + \frac{1}{2} \right) {}_1F_1 \left( m + \frac{1}{2}, 2; -\frac{R^2}{\lambda^2} \right). \quad (\text{A5})$$

Taking into account that

$$\frac{R^2}{\lambda^2} = \frac{\pi n_s R^2}{\pi n_s \lambda^2} = \frac{N}{\nu} = N\beta \quad (\text{A6})$$

and

$$\frac{a_0}{\lambda} = \sqrt{\frac{\pi n_s a_0^2}{\pi n_s \lambda^2}} = \sqrt{\frac{1}{\nu}} = \sqrt{\beta} \quad (\text{A7})$$

I get the formula (38) in the main text.

## 2. Maximum density droplet state

In the case of the MDD state the matrix elements (38) of the background-electron interaction energy can be transformed further. In this case  $\beta = 1/\nu = 1$ , and one has only one state  $|s\rangle = |\Psi_{\text{mdd}}\rangle = |0, 1, \dots, N-1\rangle$ , so that  $L_j^{\text{mdd}} = j-1$ . Then Eq. (A5) gives

$$\frac{\langle \Psi_{\text{mdd}} | \hat{V}_{be} | \Psi_{\text{mdd}} \rangle}{N e^2 / a_0} = - \sum_{j=1}^N \sum_{m=0}^{j-1} \binom{j-1}{m} \frac{(-1)^m}{m!} \Gamma \left( m + \frac{1}{2} \right) {}_1F_1 \left( m + \frac{1}{2}, 2; -N \right). \quad (\text{A8})$$

First I change the order of summation over  $j$  and  $m$ ,

$$\frac{\langle \Psi_{\text{mdd}} | \hat{V}_{be} | \Psi_{\text{mdd}} \rangle}{N e^2 / a_0} = - \sum_{m=0}^{N-1} \frac{(-1)^m}{m!} \Gamma \left( m + \frac{1}{2} \right) {}_1F_1 \left( m + \frac{1}{2}, 2; -N \right) \sum_{j=m+1}^N \binom{j-1}{m}. \quad (\text{A9})$$

The sum of binomial coefficients here gives

$$\sum_{j=m+1}^N \binom{j-1}{m} = \binom{N}{m+1}. \quad (\text{A10})$$

Second, I substitute into (A9) the definition of the hypergeometric function

$${}_1F_1(a, b; z) = \sum_{k=0}^{\infty} \frac{(a)_k}{(b)_k} \frac{z^k}{k!}, \quad (\text{A11})$$

where  $(a)_k = \Gamma(a+k)/\Gamma(a)$  is the Pochhammer symbol, and use the fact that  $\Gamma(k+2) = (k+1)!$ . After some simplifications I obtain

$$\frac{\langle \Psi_{\text{mdd}} | \hat{V}_{be} | \Psi_{\text{mdd}} \rangle}{N e^2 / a_0} = - \sum_{m=0}^{N-1} \frac{(-1)^m}{m!} \binom{N}{m+1} \sum_{k=0}^{\infty} \frac{(-N)^k}{k!(k+1)!} \Gamma \left( m + k + \frac{1}{2} \right). \quad (\text{A12})$$

Third, I change the order of summation over  $k$  and  $m$ ,

$$\frac{\langle \Psi_{\text{mdd}} | \hat{V}_{be} | \Psi_{\text{mdd}} \rangle}{N e^2 / a_0} = - \sum_{k=0}^{\infty} \frac{(-N)^k}{k!(k+1)!} \sum_{m=0}^{N-1} \frac{(-1)^m}{m!} \binom{N}{m+1} \Gamma \left( m + k + \frac{1}{2} \right) \quad (\text{A13})$$

and take the sum over  $m$ ,

$$\sum_{m=0}^{N-1} \frac{(-1)^m}{m!} \binom{N}{m+1} \Gamma\left(m+k+\frac{1}{2}\right) = \frac{\Gamma\left(k+\frac{1}{2}\right) \Gamma\left(N-k+\frac{1}{2}\right)}{\Gamma\left(\frac{3}{2}-k\right) \Gamma(N)}. \quad (\text{A14})$$

Then, using the properties of the  $\Gamma$  function,

$$\Gamma(z+1) = z\Gamma(z), \quad \Gamma\left(\frac{1}{2}+k\right) \Gamma\left(\frac{1}{2}-k\right) = \frac{\pi}{\cos \pi k} \quad (\text{A15})$$

I obtain

$$\frac{\langle \Psi_{\text{mdd}} | \hat{V}_{be} | \Psi_{\text{mdd}} \rangle}{Ne^2/a_0} = \frac{2}{\pi \Gamma(N)} \sum_{k=0}^{\infty} \frac{N^k}{k!(k+1)!} \frac{\Gamma^2\left(k+\frac{1}{2}\right) \Gamma\left(N-k+\frac{1}{2}\right)}{(2k-1)}. \quad (\text{A16})$$

The series here can be presented in the form

$$\sum_{k=0}^{\infty} \frac{N^k}{k!(k+1)!} \frac{\Gamma^2\left(k+\frac{1}{2}\right) \Gamma\left(N-k+\frac{1}{2}\right)}{(2k-1)} = -\pi \Gamma\left(N+\frac{1}{2}\right) {}_2F_2\left(-\frac{1}{2}, \frac{1}{2}; 2, \frac{1}{2}-N; -N\right), \quad (\text{A17})$$

so that finally I obtain

$$\frac{\langle \Psi_{\text{mdd}} | \hat{V}_{be} | \Psi_{\text{mdd}} \rangle}{Ne^2/a_0} = -2 \frac{\Gamma\left(N+\frac{1}{2}\right)}{\Gamma(N)} {}_2F_2\left(-\frac{1}{2}, \frac{1}{2}; 2, \frac{1}{2}-N; -N\right). \quad (\text{A18})$$

This formula is used in the main text, Eq. (69). Calculations in this Section have been done with the help of Wolfram Mathematica, <https://www.wolfram.com/mathematica>.

## Appendix B: Integrals $\mathcal{K}$

Consider the integrals

$$\mathcal{I}(n_1, n_2, k) = \sqrt{\frac{8}{\pi}} \int_0^\infty dx x^{2k} L_{n_1}^k(x^2) L_{n_2}^k(x^2) e^{-2x^2}, \quad (\text{B1})$$

where  $n_1$ ,  $n_2$ , and  $k$  are integers, and  $L_n^l(x)$  are Laguerre polynomials. Substituting the explicit expression for the generalized Laguerre polynomial (A2) into the definition (B1) I get a finite sum of integrals of the type  $\int_0^\infty x^{2n} e^{-ax^2} dx$ , which can be analytically calculated. The final result for the integrals  $\mathcal{I}$  is

$$\mathcal{I}(n_1, n_2, k) = \frac{1}{\sqrt{\pi}} \sum_{m_1=0}^{n_1} \binom{n_1+k}{m_1+k} \frac{(-1)^{m_1}}{m_1!} \sum_{m_2=0}^{n_2} \binom{n_2+k}{m_2+k} \frac{(-1)^{m_2}}{m_2!} \frac{\Gamma(m_1+m_2+k+\frac{1}{2})}{2^{m_1+m_2+k}}. \quad (\text{B2})$$

The functions  $\mathcal{K}(n_1, n_2, k)$  which determines the matrix elements of the electron-electron interaction energy (Section II E 5) are related to the integrals  $\mathcal{I}$ ,

$$\mathcal{K}(n_1, n_2, k) = \sqrt{\frac{n_1!}{(n_1+k)!} \frac{n_2!}{(n_2+k)!}} \mathcal{I}(n_1, n_2, k). \quad (\text{B3})$$

Calculations of the matrix elements of the electron-electron interaction have been also performed in Ref. [14].

## Appendix C: Supplementary Materials

The directory **Supplementary Materials** supplied together with the paper contains seven subdirectories **Nx**, where  $x$  denotes the number of particles  $N = 2, \dots, 8$ . Each subdirectory has five files (except the subdirectory **N8** that has four files). These files contain the following information:

1. The file `Nmbs.Nx.Ltotyy.dat` contains a single number, which is the number of many-body states  $N_{mbs}$  for given  $N$  and  $\mathcal{L} = 3N(N-1)/2$ .  $yy$  is a two-digit number corresponding to  $\mathcal{L}$ . Example: the file `Nmbs.N7.Ltot63.dat` contains the number  $N_{mbs} = 8033$ .
  2. The file `MBstates.Nx.Ltotyy.dat` contains  $N_{mbs}$  many-body states  $|s\rangle$ . Example: the file `MBstates.N7.Ltot63.dat` has 8033 lines containing the many-body states running from the state number 1,  $|0, 1, 2, 3, 4, 5, 48\rangle$ , up to the state number 8033,  $|6, 7, 8, 9, 10, 11, 12\rangle$ .
  3. The file `LaughlinCs.Nx.Ltotyy.dat` contains the integer numbers  $C_s^{\text{RL}}$  obtained using the binomial expansion of the polynomial factors in the Laughlin function (79), see Section V B. Example: the first and the last lines in the file `LaughlinCs.N7.Ltot63.dat` contain the numbers  $C_{|0,1,2,3,4,5,48\rangle} = 0$  and  $C_{|6,7,8,9,10,11,12\rangle} = 135135$ .
  4. The file `LaughlinAs.Nx.Ltotyy.dat` contains the real expansion coefficients  $A_s^{\text{RL}}$ , Eq. (90), of the Laughlin function over the basis many-body states, see Section V B.
  5. The file `GrStateAs.Nx.Ltotyy.dat` contains the real expansion coefficients  $A_s^{\text{GS}}$  of the ground state function over the basis many-body states, i.e. the eigenvector of the Hamiltonian corresponding to the lowest energy eigenvalue. The subdirectory `N8` does not contain this file.
- 

- [1] K. von Klitzing, G. Dorda, and M. Pepper, New method for high-accuracy determination of the fine-structure constant based on quantized Hall resistance, *Phys. Rev. Lett.* **45**, 494 (1980).
- [2] R. E. Prange and S. M. Girvin, eds., *The Quantum Hall Effect* (Springer, New York, 1990).
- [3] D. C. Tsui, H. L. Stormer, and A. C. Gossard, Two-dimensional magnetotransport in the extreme quantum limit, *Phys. Rev. Lett.* **48**, 1559 (1982).
- [4] R. Willett, J. P. Eisenstein, H. L. Stormer, D. C. Tsui, A. C. Gossard, and J. H. English, Observation of an even-denominator quantum number in the fractional quantum Hall effect, *Phys. Rev. Lett.* **59**, 1776 (1987).
- [5] E. Wigner, On the interaction of electrons in metals, *Phys. Rev.* **46**, 1002 (1934).
- [6] R. B. Laughlin, Anomalous quantum Hall effect: An incompressible quantum liquid with fractionally charged excitations, *Phys. Rev. Lett.* **50**, 1395 (1983).
- [7] Y. A. Bychkov, S. V. Iordanskii, and G. M. Eliashberg, Two-dimensional electrons in a strong magnetic field, *JETP Lett.* **33**, 143 (1981).
- [8] D. Yoshioka and H. Fukuyama, Charge density wave state of two-dimensional electrons in strong magnetic fields, *J. Phys. Soc. Japan* **47**, 394 (1979).
- [9] D. Yoshioka and P. A. Lee, Ground-state energy of a two-dimensional charge-density-wave state in a strong magnetic field, *Phys. Rev. B* **27**, 4986 (1983).
- [10] R. Tao, Comment on Laughlin's wavefunction for the quantised Hall effect, *J. Phys. C: Solid State Phys.* **17**, L53 (1984).
- [11] K. Maki and X. Zotos, Static and dynamic properties of a two-dimensional Wigner crystal in a strong magnetic field, *Phys. Rev. B* **28**, 4349 (1983).
- [12] D. Yoshioka, B. I. Halperin, and P. A. Lee, Ground state of two-dimensional electrons in strong magnetic fields and 1/3 quantized Hall effect, *Phys. Rev. Lett.* **50**, 1219 (1983).
- [13] <https://www.nobelprize.org/prizes/physics/1998/summary/>.
- [14] S. M. Girvin and T. Jach, Interacting electrons in two-dimensional Landau levels: Results for small clusters, *Phys. Rev. B* **28**, 4506 (1983).
- [15] F. D. M. Haldane, *Phys. Rev. Lett.* **51**, 605 (1983).
- [16] D. Levesque, J. J. Weis, and A. H. MacDonald, Crystallization of the incompressible quantum-fluid state of a two-dimensional electron gas in a strong magnetic field, *Phys. Rev. B* **30**, 1056 (1984).
- [17] J. K. Jain, Composite-fermion approach for the fractional quantum Hall effect, *Phys. Rev. Lett.* **63**, 199 (1989).
- [18] M. Kasner and W. Apel, Electrons in a strong magnetic field on a disk, *Annalen der Physik* **3**, 433 (1994).
- [19] R. H. Morf, N. d'Ambrumenil, and S. Das Sarma, Excitation gaps in fractional quantum Hall states: An exact diagonalization study, *Phys. Rev. B* **66**, 075408 (2002).
- [20] O. Ciftja and C. Wexler, Monte Carlo simulation method for Laughlin-like states in a disk geometry, *Phys. Rev. B* **67**, 075304 (2003).
- [21] O. Ciftja, C. M. Lapilli, and C. Wexler, Liquid crystalline states for two-dimensional electrons in strong magnetic fields, *Phys. Rev. B* **69**, 125320 (2004).
- [22] O. Ciftja, N. Ockleberry, and C. Okolo, One-particle density of Laughlin states at finite  $N$ , *Mod. Phys. Lett. B* **25**, 1983 (2011).
- [23] V. J. Goldman and B. Su, Resonant tunneling in the quantum Hall regime: Measurement of fractional charge, *Science* **267**, 1010 (1995).
- [24] L. Saminadayar, D. C. Glattli, Y. Jin, and B. Etienne, Observation of the  $e/3$  fractionally charged Laughlin quasiparticle, *Phys. Rev. Lett.* **79**, 2526 (1997).

- [25] R. de-Picciotto, M. Reznikov, M. Heiblum, V. Umansky, G. Bunin, and D. Mahalu, Direct observation of a fractional charge, *Nature* **389**, 162 (1997).
- [26] J. P. Eisenstein and H. L. Stormer, The fractional quantum Hall effect, *Science* **248**, 1510 (1990).
- [27] J. Jain, ed., *Composite Fermions* (Cambridge University Press, Cambridge, 2012).
- [28] T. H. Hansson, M. Hermanns, S. H. Simon, and S. F. Viefers, Quantum Hall physics: Hierarchies and conformal field theory techniques, *Rev. Mod. Phys.* **89**, 025005 (2017).
- [29] G. Murthy and R. Shankar, Hamiltonian theories of the fractional quantum Hall effect, *Rev. Mod. Phys.* **75**, 1101 (2003).
- [30] S. A. Mikhailov and K. Ziegler, Floating Wigner molecules and possible phase transitions in quantum dots, *European Physical Journal B* **28**, 117 (2002).
- [31] C. Yannouleas and U. Landman, Two-dimensional quantum dots in high magnetic fields: Rotating-electron-molecule versus composite-fermion approach, *Phys. Rev. B* **68**, 035326 (2003).
- [32] C. Yannouleas and U. Landman, Symmetry breaking and quantum correlations in finite systems: studies of quantum dots and ultracold Bose gases and related nuclear and chemical methods, *Rep. Prog. Phys.* **70**, 2067–2148 (2007).
- [33] M. Lewin, E. H. Lieb, and R. Seiringer, Statistical mechanics of the uniform electron gas, *Journal de l’École polytechnique — Mathématiques* **5**, 79 (2018).
- [34] M. Lewin, E. H. Lieb, and R. Seiringer, Floating Wigner crystal with no boundary charge fluctuations, *Phys. Rev. B* **100**, 035127 (2019).
- [35] A. P. Prudnikov, Y. A. Brychkov, and O. I. Marichev, *Integrals and Series, Special functions*, Vol. 2 (Nauka, Moscow, 1983).